# Vascular density and distribution in neocortex

Schmid, Franca ; Barrett, Matthew J P ; Jenny, Patrick ; Weber, Bruno

Abstract: An amazingly wide range of complex behavior emerges from the cerebral cortex. Much of the information processing that leads to these behaviors is performed in neocortical circuits that span throughout the six layers of the cortex. Maintaining this circuit activity requires substantial quantities of oxygen and energy substrates, which are delivered by the complex yet well-organized and tightly-regulated vascular system. In this review, we provide a detailed characterization of the most relevant anatomical and functional features of the cortical vasculature. This includes a compilation of the available data on laminar variation of vascular density and the topological aspects of the microvascular system. We also review the spatio-temporal dynamics of cortical blood flow regulation and oxygenation, many aspects of which remain poorly understood. Finally, we discuss some of the important implications of vascular density, distribution, oxygenation and blood flow regulation for (laminar) fMRI.

DOI: https://doi.org/10.1016/j.neuroimage.2017.06.046

# Vascular density and distribution in neocortex

Franca Schmid[1], Matthew J.P. Barrett[2,3], Patrick Jenny[1], Bruno Weber[2,3]

1. Institute of Fluid Dynamics, ETH Zurich, Sonneggstrasse 3, 8092 Zurich, Switzerland
2. Institute of Pharmacology and Toxicology, University of Zurich, Winterthurerstrasse 190, CH-8057 Zurich, Switzerland
3. Neuroscience Center, University and ETH Zurich, Winterthurerstrasse 190, CH-8057 Zurich, Switzerland

*Corresponding author:* Franca Schmid, schmid@ifd.mavt.ethz.ch

**Abstract**

An amazingly wide range of complex behavior emerges from the cerebral cortex. Much of the information processing that leads to these behaviors is performed in neocortical circuits that span throughout the six layers of the cortex. Maintaining this circuit activity requires substantial quantities of oxygen and energy substrates, which are delivered by the complex yet well-organized and tightly-regulated vascular system. In this review, we provide a detailed characterization of the most relevant anatomical and functional features of the cortical vasculature. This includes a compilation of the available data on laminar variation of vascular density and the topological aspects of the microvascular system. We also review the spatio-temporal dynamics of cortical blood flow regulation and oxygenation, many aspects of which remain poorly understood. Finally, we discuss some of the important implications of vascular density, distribution, oxygenation and blood flow regulation for (laminar) fMRI.

Keywords: cortical microvasculature, vascular density, neurovascular coupling, hemodynamic response, cerebral oxygenation, laminar characteristics

## 1 Introduction

The brain consumes approximately a quarter of the body's total glucose and a fifth of the oxygen, an order of magnitude more than what would be expected on a weight basis. This remarkable energy demand requires a robust energy supply via the blood stream, and a complex cerebrovascular system has evolved to meet this demand. A detailed knowledge of the cerebral vasculature is crucial to understand the basic principles of cerebral blood flow (CBF), its coupling to neural processing, and also to understand non-invasive human brain imaging. Given the extraordinary importance of structural and functional magnetic resonance imaging (fMRI), it is quite surprising that quantitative data regarding cerebral blood vessels are sparse. In particular, the microvascular system is significantly understudied both in terms of its structural and functional characteristics. The aim of the present review is to provide a detailed overview of the cerebral microvascular system, with a focus on the neocortex and its importance for laminar MRI.

The human brain receives approximately 15-20% of the total cardiac output and this blood is transported from the trunk via four large vessels, the left and right internal carotid arteries and the left and right vertebral arteries. Before ramifying into the large feeding arteries of the brain, the vertebral arteries join into the basal artery and together with the carotid vessels form a ring-like structure called the circle of Willis. This structure introduces redundancy and serves as a precautionary measure. The middle cerebral artery's circulation territory is the largest and comprises large parts of the frontal, temporal and parietal cortex. Without being too detailed, the posterior cerebral artery feeds the inferior and medial surface of the occipital and temporal cortices, whereas the anterior cerebral artery is responsible for the perfusion of medial aspects of the frontal and parietal cortex. Whereas the feeding territories of the large cerebral arteries play an important role in the diagnosis of neurological disorders, they have only a minor importance for cortical MRI. Of much greater importance is the cerebral microvasculature and hence this review will be focused

on the mammalian cortical microvasculature (for a recent review, please also see Hirsch et al., 2012).
The main duty of the cerebrovascular system is to deliver oxygen and glucose to the tissue. The human brain metabolizes about 31 mmol glucose per 100 grams of tissue per minute to produce adenosine-triphosphate (ATP), which is to a large extent formed by oxidative phosphorylation in the tricarboxylic acid cycle. This metabolic pathway requires a large amount of oxygen, which diffuses from microvessels to mitochondria of the brain cells. Within the blood vessels, chemically bound oxygen molecules dissociate from hemoglobin and dissolved oxygen diffuses through the red blood cell membrane, blood plasma, the capillary wall, and interstitial fluid until it enters the neurons and glial cells, where it is metabolized. Blood-borne glucose travels along the same route; however, in contrast to oxygen, which can freely diffuse, glucose molecules are transported across membranes with the help of glucose transporters. A major waste product of brain energy metabolism is $CO_2$, which rapidly diffuses out of the nervous tissue and is cleared from the brain also via the vascular system. The brain vascular system is not only responsible for supply and waste collection, but also acts as a barrier that restricts the passage of molecules from blood to brain. The endothelial cells of the brain vessels are coupled by tight junctions and form the blood-brain barrier.
It was recognized as early as the 19$^{th}$ century that the brain's blood supply is dynamic, and that changes in neural activity are mirrored by precisely controlled changes in hemodynamics (Mosso, 1881; Roy and Sherrington, 1890). This spatial and temporal neurovascular coupling has been systematically used to generate detailed maps of hemodynamic changes that are assumed to be surrogates of the actual regional neural activation. The most important application of this relationship is the so-called blood oxygenation level-dependent (BOLD) contrast (Kwong et al., 1992; Ogawa et al., 1990) used in fMRI.
The neocortex is one of the most intriguing structures of the brain. It shows an extraordinary flexibility, given the large range of behavior that emerges despite only limited variation in its anatomical organization across the different cortical areas (Douglas and Martin, 2004). The laminar organization of the cortex and its impact on structural and functional MRI is the topic of this special issue. The six-layered structure, with well-defined microcircuits (Douglas and Martin, 2004), is largely preserved across species. Similarly, the vascular system of the neocortex also shows a high degree of organization throughout the cortical depth, an organization that is analogous in all the studied animal models as well as in the human cortical microvasculature.
The present review introduces the vascular system of the neocortex and is structured in the following way. After a short explanation of the most important methods used to investigate brain blood vessels, we introduce the gross organization followed by a detailed characterization of laminar density variation, topological aspects, and flow regulation of the microvascular system. We end the review with a discussion of the relevance of the vasculature system for (laminar) fMRI.

## 2 Methods to study brain vasculature

Classical studies of the microvascular network are based on Indian ink fillings and scanning electron microscopy of vascular corrosion casts (Duvernoy et al., 1981; Reina-De La Torre et

al., 1998; Weber et al., 2008). The combination of immunohistochemistry and stereology also allows estimating vessel diameters and vascular density (Weber et al., 2008).
However, the three-dimensional vascular network topology of the neocortex has not been studied in detail until recently, when new technologies became available. In order to describe the network in three dimensions, methods are required that have a spatial resolution to resolve capillaries in a sufficiently large field of view to cover an entire cortical column. In order to estimate the diameter of capillaries, submicron spatial resolution is required. David Kleinfeld and colleagues have developed the so-called all-optical histology technique (Tsai et al., 2003; Tsai et al., 2009), whereby two-photon microscopy is used to image the fluorescently labeled vasculature, and laser ablation is used to increase the field of view, which would normally be limited to a few hundred micrometers. Another possible approach is the use of synchrotron radiation-based X-ray microscopy, where a high photon flux is exploited to acquire absorption-based tomographic images of the vasculature (Guibert et al., 2010; Heinzer et al., 2006; Plouraboue et al., 2004; Reichold et al., 2009). Recently, the classical Indian ink filling method has been combined with a serial section microscopic technique, called Micro-Optical Sectioning Tomography (MOST), and was used to acquire the vascular system of the entire mouse brain (Xue et al., 2014).
With the advent of advanced tissue clearing methods, selective plane illumination microscopy (SPIM) or ultramicroscopy (Erturk et al., 2012) is becoming an increasingly powerful approach to acquire and reconstruct fluorescently labeled vessels in large samples. To date, the spatial resolution and a varying point spread function across the field of view are technical challenges that need to be overcome for the method to become a novel standard.
All the histological techniques share the problem of tissue deformation, either due to fixation and/or clearing of the tissue. Therefore, measurements of the microvascular network need to be corrected for these alterations. One way of doing this is to measure vascular diameters in vivo using two-photon microscopy and to use the diameter distribution to transform the ex vivo measurements (Tsai et al., 2009). Moreover, future studies could deploy deep in vivo two-photon microscopy to acquire the cortical vascular system in its entire depth.

## 3 Gross structure of the cortical vascular system

The cerebral arteries run along the surface of the cortex and ramify into a complex network of so-called pial arteries. These arteries are situated in the subarachnoid space and are surrounded by a pial cell lining. The topology of this pial arterial network ensures a robust delivery of blood to the cerebral cortex (Section 5.1).
Once an artery leaves the pial network, it penetrates perpendicularly into the cortex (Figure 1). The pial cell ensheathment of the arteries continues in the form of a perivascular channel (Zhang et al., 1990). This pial cell layer is perforated at the arteriolar level and is completely absent on capillaries and veins. A perivascular space, termed the Virchow-Robin space, surrounds the cortical arteries and veins in a funnel-shaped manner. Around the large pial and diving vessels, astrocytes define the Virchow-Robin space. This perivascular space is a clearing route for interstitial solutes, much as the lymphatic system is for the rest of the body (Iliff and Nedergaard, 2013; Iliff et al., 2012; Iliff et al., 2013; Xie et al., 2013). This so-called glymphatic system consists of a para-arterial influx route; a para-venous clearance

route; and a trans-parenchymal pathway depending on the aquaporin-4 water channel in astrocytes.
The cortical arteries send off collaterals at different cortical depths. This fact led to the introduction of a classification scheme by Duvernoy et al. (1981), in which a vessel of type 1 would feed/drain superficial cortical layers, whereas higher order vessel types would feed/drain deeper layers. Some cortical arteries even penetrate the entire cortex without any collateral until reaching white matter (Section 5.2). It is important to note that these classes are not completely separable, but appear rather as a continuum. Cortical arteries diverge into arterioles (small arteries) and eventually end in the capillary network (Section 5.3). The capillary network, where most of the exchange of energy substrates and oxygen occurs between blood and tissue, converges into the venous system. Again, principal cortical veins are oriented perpendicularly to the cortical surface (Section 5.2). The basic building principle of the cortical vasculature is, therefore, delivery of blood from the cortical surface, penetration into the cortex in a perpendicular manner and, after the capillary passage, drainage back to the surface, where the blood is eventually transported away via the venous system that converges into large sinuses.
There are distinct differences in the ultrastructure between the different types of cerebral blood vessels. Common to arteries, capillaries and veins are the endothelial cell layer and the thin basal membrane. Endothelial cells are coupled by tight junctions and form the blood-brain barrier that restricts the passage of molecules from blood to brain. Whereas capillaries only consist of these two elements, arteries and to a much lesser extent also veins are covered with a smooth muscle sheath. These smooth muscles are responsible for regulating the vascular resistance by changing the vessel diameter (Section 6). Pericytes are a very heterogeneous cell type that have a claw-like appearance and are located on the abluminal side of endothelial cells (Armulik et al., 2011). They also have a contractile capacity, but their role as active regulators of vascular resistance is debated (Section 6, (Fernandez-Klett et al., 2010; Hall et al., 2014; Hamilton et al., 2010; Peppiatt et al., 2006)). Furthermore, all microvessels are almost completely covered by astrocytic endfeet (Mathiisen et al., 2010). This perivascular astrocytic sheath is thought to play a pivotal role in the transcellular trafficking of metabolites as well as water and ion exchange at the blood-brain interface.

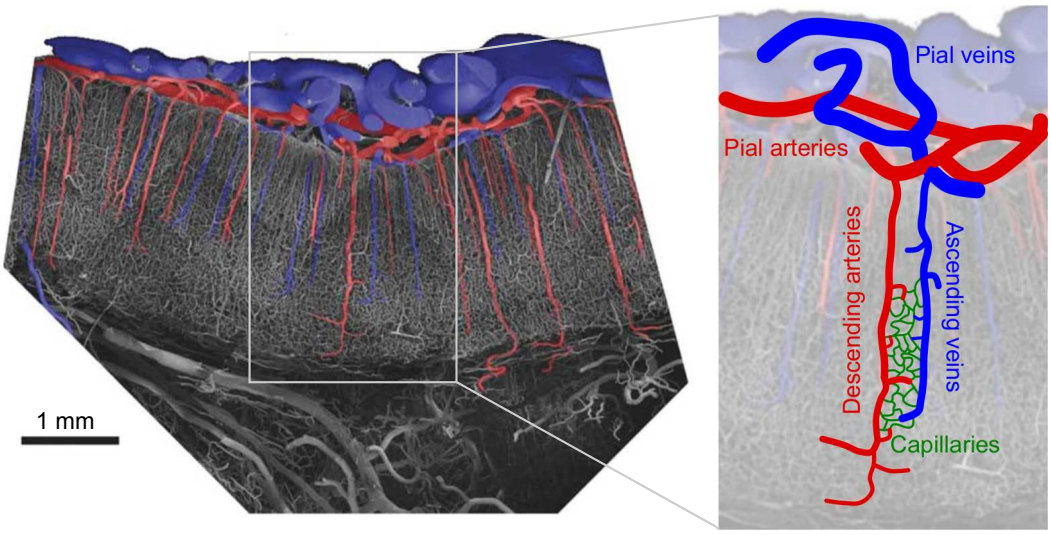

Figure 1 Gross structure of the cortical vasculature. Left: Scanning electron micrograph of a vascular corrosion cast from the monkey visual cortex (primary visual cortex). Arteries are shaded in red and veins are blue. Figure from Hirsch et al. (2012). Right: Schematic representation of the cortical vasculature and its key components.

## 4 Density of the cortical microvascular system

The diameters of cortical vessels range from around 4 μm (capillaries) to a few tens of microns (arteries/veins) (Blinder et al., 2013; Duvernoy et al., 1981; Gutiérrez-Jiménez et al., 2016; Hall et al., 2014; Tsai et al., 2009; Weber et al., 2008). When looking at the distribution of the calibers, it becomes obvious that the most frequent vessel type is the capillary, irrespective of the species (Weber et al., 2008). The capillary network can be regarded as a redundant network with a mesh width of approximately 50 μm (Section 5.3). This mesh width is probably adjusted to the diffusion constant of oxygen in brain tissue. The overall vascular volume fraction ranges between 1 and 3% of the total brain volume, depending on the species and the applied method (Blinder et al., 2013; Lauwers et al., 2008; Risser et al., 2009; Tsai et al., 2009; Weber et al., 2008). Although similar vascular network characteristics can be found throughout the cortex, there are variations, both across the cortical layers and between different cortical areas (Figure 2). In the primary sensory areas, the highest vascular density can be found in layer IV. This is most obvious in the primate primary visual cortex, where layer IVcβ displays an increase in vascular density that is easily detectable (Fonta and Imbert, 2002; Weber et al., 2008).

Several authors have investigated the relationship between vascular and neuronal density, but the evidence suggests that the relationship is weak (Tsai et al., 2009; Weber et al., 2008). In the macaque cortex, this correlation was particularly weak in the upper layers of cortex (Weber et al., 2008). However, a much stronger correlation between the pattern of oxidative metabolism and microvascular density was observed (Keller et al., 2011; Weber et al., 2008).

The Kleinfeld group has studied the mouse barrel cortex and found that the variation in cellular density across the cortical depth was more pronounced than that of the vascular density (Tsai et al., 2009). Moreover, the vascular radius distribution was very similar across the cortical depth. If we look at the microvascular density along the cortical layers in the primary visual cortex, there is a marked gradient with the highest density in layer IVc-β (Weber et al., 2008; Zheng et al., 1991).

From a developmental perspective, Fonta and Imbert (2002) were able to demonstrate that the relative vascular density developed in parallel to cytochrome oxidase activity and was highest in layer IVc-α in the first postnatal month. (Cytochrome oxidase activity is a histochemical procedure to assess the oxidative metabolic demand of a given brain region.) In the next developmental phase, the vascular density and cytochrome oxidase activity in the two layers are similar, before layer IVc-β eventually becomes the most densely vascularized layer. In the cat, a similar change in steady-state metabolic demand and vascular density was observed. It was found that layer IV in the cat striate area 17 showed the highest relative vascular density and relative glucose utilization. However, this laminar difference could only be found in the adult but not in 5-week-old kittens (Tieman et al., 2004). Changes in vascular organization can also be observed in the adult animal. Whereas acute hypoxia is compensated with an increase in CBF, prolonged hypoxia leads to a marked

increase in capillary density (Diemer and Henn, 1965; Harik et al., 1994; LaManna et al., 1992; Miller and Hale, 1970; Opitz, 1951).
Weber and colleagues stereologically determined vascular density values on the basis of anti-collagen immunohistochemistry from a large number of samples from the macaque visual cortices V1, V2, V3 and V4 (Weber et al., 2008). The authors found that the overall vascular length density in visual gray matter lay around 478 $mm/mm^3$, whereas the volume fraction was approximately 2.1 %. As elaborated above, the vascular network of the striate cortex also displays a special laminar organization. The volume fraction and length density in layer IVc-$\beta$ were 2.70 % and 627.83 $mm/mm^3$ respectively. The lowest vascular length density was found in layer I (408.44 $mm/mm^3$), whereas layer II showed the lowest volume fraction (1.93 %). These superficial density data coincide with the relatively low cell body density and high proportion of myelinated and unmyelinated fibers in layer I and II. The vascular data from V2, V3 and V4 were very similar, with layer IV showing the highest density (volume fraction 2.18%) and layer VI the lowest (volume fraction 2.01%). It is important to note, that different vessel calibers contribute differentially to the different vascular density metrics. When focusing on the mere length as in length density, it is obvious that by far the largest contribution is provided by the capillaries. However, for other quantities the contribution of the non-capillaries may be higher, according to their respective dependence on the vessel radius. (The length density's dependence on the vessel diameter is $d^0$, that of the surface density is $d^1$ and that of the volume fraction is $d^2$.) Due to the volume fraction's quadratic dependence on the diameter, the contribution of large vessels surpasses that of the capillaries, despite their much lower frequency (Figure 2).
The primary visual cortex seems to be unique with respect to the microvascular system as well, since overall vascular density is clearly higher in the striate cortex than in the extra-striate cortices (Fonta and Imbert, 2002; Tieman et al., 2004; Zheng et al., 1991). However, differences between the extra-striate areas are small or even negligible (Weber et al., 2008). The vascular density differences between the primary and non-primary areas were also found in the somatosensory and auditory cortex, and the vascular densities of the secondary auditory and somatosensory areas were comparable to those of the extrastriate cortex (own unpublished observations). Taken together, it seems that non-primary cortical areas share a similar microvascular architecture. Therefore, based on the vascular structure alone, it appears that large differences in the hemodynamic response and laminar MRI are not to be expected within these areas. However, caution is advised when hemodynamic response patterns are directly compared between primary and non-primary areas (Section 8).
It is surprising that we do not see significant differences in the vascular density of large vessels over cortical depth, despite the fact that Duvernoy et al. (1981) states that DAs and AVs of group 4 (Table 1) are the most frequent group of penetrating trees. First of all, it should be noted that Duvernoy's classification has been derived for the vasculature of the human brain and thus species dependent differences might exist. Furthermore, differences in vessel diameter for different groups of penetrating trees might blur those characteristics. In addition to the overall vascular density, the relative volume fraction occupied by blood vessels of different categories, i.e. arteries, capillaries and veins, is relevant for many applications. For example, the fraction of blood found in the different vessel types is an important parameter in compartmental biophysical models.
The measurements from the macaque visual cortex discussed above estimated that capillaries (defined as vessels with diameter < 8 µm) made up approximately 41 % of the

total vascular volume fraction (Weber et al., 2008). This is similar to an estimate of ~48 % obtained from Indian ink injected sections of human cortex, which were taken from the fusiform and parahippocampal gyri (Lauwers et al., 2008). While there is a range of microvascular data comparing the relative number of descending arteries (DAs) and ascending veins (AVs, Section 5.2), to our knowledge no such data exist describing the distribution of blood volume between arterial and venous compartments. However, it is possible to use data from a range of lower resolution techniques such MRI and PET, and based on this approach Barrett et al. (2012) estimated arteries make up ~29 % of total blood volume, and veins contribute ~27 %, using mostly human and primate data.

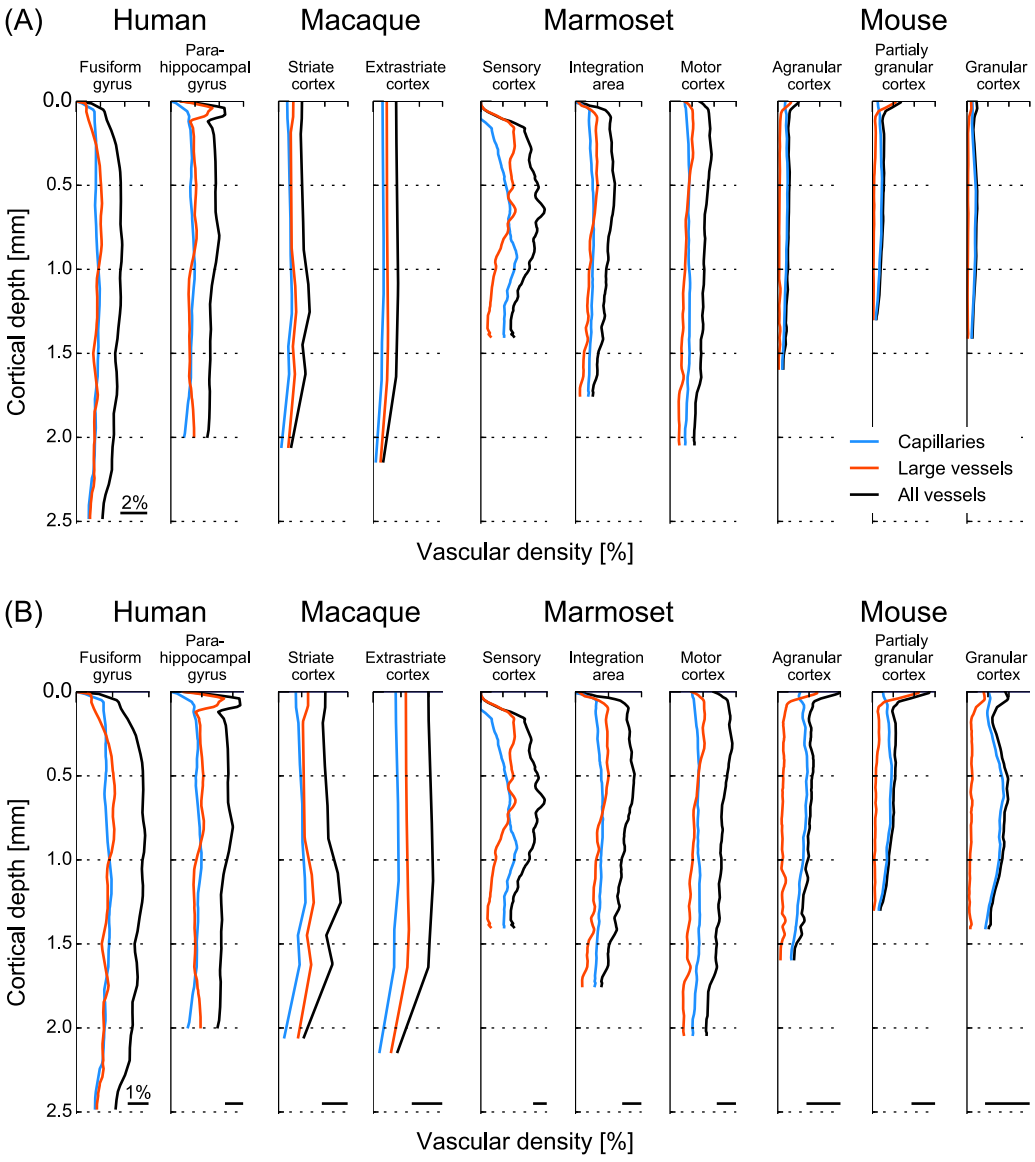


Figure 2 Vascular density of the cortical depth. Vascular density over cortical depth for different species, different areas and different vessel types with similar (A) and different (B) x-axes scales. Data from: Lauwers et al. (2008) (Human); Weber et al. (2008) (Macaque); Risser et al. (2009) (Marmoset); Tsai et al. (2009) (Mouse). The cut-off diameter to differentiate between capillaries and large vessels differs for different species. Here, the following values were used: Human: 10 µm, Macaque: 6 µm, Marmoset: 11.2 µm, Mouse 6 µm.

## 5 Topological aspects of the cortical vascular system

In Section 3 we introduced the gross anatomical structure of the cortical vasculature consisting of pial and penetrating vessels and the capillary bed. Here, we focus on specific topological characteristics and on the role of the three vessel types in the distribution of blood. A profound knowledge of the vascular topology is relevant not only for understanding neurovascular coupling but also to comment on the severity of vessel occlusion at different locations. Unless stated otherwise the described characteristics are valid across species.

### 5.1 The pial network

The pial network is a 2-D-planar network located at the cortical surface. The pial arteries distribute blood from the large cerebral arteries to the intracortical vessels and the pial veins collect it.
As the pial arteries are at the beginning of the pathway of blood through the cortex, a robust network topology, which guarantees a constant supply of blood, is crucial. This is achieved by a large number of arterial anastomoses, which on average contain four edges (Blinder et al., 2010; Duvernoy et al., 1981; Schaffer et al., 2006). Overall, the structure of the pial arterial network is comparable to that of a honeycomb (Blinder et al., 2010).
For a thorough analysis of the redundancies at the pial level, Blinder et al. (2010) introduce the concept of the backbone of the pial network (Figure 3A). The backbone spans the whole territory of the pial network, even though it is made up of only ~11% of the pial arteries. In addition, nearly 75% of all descending arteries (DAs) start at a backbone edge. This property further increases the robustness, because two different pial vessels can feed those arteries.
Occlusion experiments have demonstrated the robustness of the pial network (Blinder et al., 2010; Schaffer et al., 2006). Schaffer et al. (2006) showed that single vessel occlusion induces a redistribution of flow with the positive effect that all vessels stay perfused (Figure 3F). Nonetheless, the flow rates in individual vessels are significantly affected and flow reversals, reductions and even increases are observed (Schaffer et al., 2006). Blinder et al. (2010) noted that in low flux DAs the flow is preserved in response to pial artery occlusion, while it decreases in high flux DAs. This suggests that high flux DAs contain blood reserves that can be redistributed in case of occlusion.
The network topology of the pial veins is significantly less studied. The prevailing view is that it has fewer anastomoses than its arterial counterpart and is rather a “drainage system like a river watershed” (Adams et al., 2014). Generally, pial veins are larger in diameter than pial arterioles. Duvernoy et al. (1981) observe that in the human brain large pial veins tend to surpass the sulci and remain at the cortical surface. This is in contrast to pial arteries where the main trunk is often located within the sulci. Furthermore, pial arteries normally run above pial veins (Duvernoy et al., 1981).

### 5.2 The penetrating vessels

The DAs deliver blood to the capillary bed over the entire depth of the cortex. After the blood passes the capillary network it is collected in the ascending veins (AVs) and returns towards the cortical surface. It is well established that DAs, as well as AVs, have a tree-like

structure and differ significantly in their penetration depth (Blinder et al., 2013; Cassot et al., 2009; Duvernoy et al., 1981; Guibert et al., 2012; Hirsch et al., 2012; Lauwers et al., 2008; Reina-De La Torre et al., 1998). The most widespread classification for penetrating vessels is by Duvernoy et al. (1981), and is summarized in Table 1. The authors proposed that different groups of DAs are responsible for feeding different cortical layers. Guibert et al. (2012) provided some evidence for this hypothesis in their numerical work, and showed that the depth of the feeding region strongly correlates with the penetration depth of the DA.

| Vessel Group | 1 | 2 | 3 | 4 | 5 | 6 |
|---|---|---|---|---|---|---|
| Penetration depth (cortical layer) | I - II | IIIa | IIIc - Va | VI | down to WM | down to WM without branching |

Table 1 Classification of penetrating vessels based on their penetration depth by Duvernoy et al. (1981). The classification is valid for DAs as well as AVs (with the exception of group 6 which only exists for DAs). All penetrating trees, with exception of group 6, have offshoots along their depth. WM: white matter.

The DAs belonging to group 4 are the most numerous (Duvernoy et al., 1981), and the number of branches feeding the capillary bed peaks at cortical layer IV (Figure 3E) (Blinder et al., 2013; Schmid et al., 2017). While this evidence suggests that the DA topology is designed with the major purpose of supplying blood to layer IV, topological characteristics alone do not predict flow. Indeed, Schmid et al. (2017) showed that, in contrast to the number of capillary starting points, the RBC influx is maximal close to the cortical surface (Figure 3E).
Of further interest is the distribution of DAs with respect to each other and to the AVs. The ratio of DAs to AVs is highly species dependent and while for primates there are more DAs than AVs, the opposite trend is observed for rodents (Table 2). The evolutionary basis for these differences remains unclear.

| Species | Human | Monkey | Rat | Mouse |
|---|---|---|---|---|
| Ratio DA : AV | 2.2 : 1 | 2.1 : 1 | 1 : 1.8 | 1 : 3.0 |
| DAs per $mm^2$ | 1.0 | 7.9 | 8.3 | 3.9 |
| AVs per $mm^2$ | 0.5 | 3.6 | 10.3 | - |

Table 2 Average ratios of DAs to AVs, average number of DAs and AVs2 for different species. References: Human: (Cassot et al., 2009; Lauwers et al., 2008); Monkey: (Adams et al., 2014; Guibert et al., 2010; Risser et al., 2009; Weber et al., 2008); Rat: (Blinder et al., 2010; Nguyen et al., 2011); Mouse: (Blinder et al., 2010; Blinder et al., 2013).

It has been hypothesized that the distribution of DAs correlates with the location of functional neuronal units, such as barrels (somatosensory cortex) or blobs (visual cortex). For the barrel cortex no such correlation could be detected (Figure 3B; Blinder et al. (2013)). For the blobs the matter remains controversial. Keller et al. (2011) observed an increased DA density between the blobs. However, this is in contrast to results from Adams et al. (2014), who did not observe any differences in the DA density.
Although there is no clear evidence supporting a strong correlation between functional units and the distribution of DAs, it seems likely that each DA is responsible for feeding a

specific tissue volume. Shih et al. (2013) occluded DAs in the rat cortex to estimate the feeding region of individual DAs. They state that the infarct volume is proportional to the baseline flux in the occluded DA and on average affects a cylindrical volume with a radius of 460 µm and a depth of 1.17 mm.
Guibert et al. (2012) determined the feeding volume based on numerical blood flow simulations in the marmoset cortex. They obtained a feeding volume with a radius of 386 µm and a depth of 2 mm. Considering the large size of the brain this value might seem comparably small. However, it should be kept in mind that the DA:AV ratio is >1 for primates while it is <1 for rodents. Furthermore, the volume measurement presented by Guibert et al. (2012) is a conservative estimate because it is defined as the volume which is exclusively fed by one DA, and not the whole volume affected by one DA. Accurate comparisons are also complex because the DA density increases with the distance to the origin of the middle cerebral artery (MCA), and consequently the feeding volume is likely to decrease (Blinder et al., 2010). Additionally, the density of penetrating vessels differs depending on cortical area (Risser et al., 2009).
The studies by Nishimura et al. (2007) and Blinder et al. (2013) further underline the crucial role of DAs in the supply of blood (Figure 3F). The effect of a DA occlusion is apparent up to ten segments from the site of occlusion (Blinder et al., 2013). There is still increased variability in RBC velocities even after a distance of 350 µm, where the mean RBC speed maintains its baseline value (Nishimura et al., 2007).
Even though evidence suggests that an AV occlusion is as critical as a DA occlusion (Shih et al., 2013), the AVs have received significantly less attention than the DAs. Nguyen et al. (2011) hypothesized that if the ratio of DAs to AVs is larger than 1 an AV occlusion is more severe and vice versa. For the marmoset, macaque and human, where the ratio of DA:AV is greater than 1, the draining region of one AV is significantly larger than the feeding region of one DA (Guibert et al., 2012; Lorthois et al., 2011, Weber et al., 2008). Furthermore, Lorthois et al. (2011) showed that the drainage volume increases with the diameter of the AV.
The diameter of the penetrating vessels is strongly species dependent. Blinder et al. (2013) state that in the mouse the mean diameter is 11 µm and 9 µm for DAs and AVs, respectively. Opposing trends have been recorded in the human brain, here the vessel diameter of AVs is larger than the one of DAs (65 µm vs. 35 µm for penetrating vessels of group 4) (Duvernoy et al., 1981). Moreover, the mean vessel diameter increases with the penetration depth of the DA/AV. Interestingly, in contrast to the DAs, the number of AV offshoots decreases with cortical depth (Blinder et al., 2013).
Relatively little is known about the relative placement of DAs and AVs. Based on the analysis of microvascular network from the mouse cortex Blinder et al. (2013) suggested a rhombic lattice where one DA is encircled by six AVs. A comparable concept was proposed by Duvernoy et al. (1981) who state that a “vascular unit” in the human brain consists of an AV surrounded by several DAs (Please bear in mind that in the human brain the DA:AV ratio approximately 2). From a sole fluid dynamical point of view it is plausible that the AVs/DAs are fed equally by the central DAs/AVs. However, opposing trends have been observed in numerical works from Guibert et al. (2012) and Schmid et al. (2017). Guibert et al. (2012) state that 61.5 % of the flow of one DA is drained into one AV. Additionally Schmid et al. (2017) observe that 72% of RBCs drained by an AV originate from one DA. Those observations can only be explained by a specific microvasculature topology or flow pattern that favors the directional flow towards one AV. Nonetheless, it has to be kept in mind that

although there seems to be a preferential AV for every DA, the DAs and AVs are highly interconnected. Indeed, Guibert et al. (2012) showed that in the marmoset one DA is connected to 22 AVs.
All in all, multiple experimental as well as numerical studies demonstrate that the penetrating vessels are crucial to maintain a sufficient supply of blood to the tissue. However, many open questions concerning their distribution and layer-specific feeding remain to be answered.

### 5.3 The capillary bed

The capillary bed has a mesh-like structure, generally described as homogeneous and highly interconnected (Blinder et al., 2013), and hence its topology is significantly more difficult to analyze than the pial vessels' or the penetrating trees' (Blinder et al., 2013; Cassot et al., 2009; Hirsch et al., 2012; Lauwers et al., 2008). Nonetheless, the flow field in the capillary bed is very heterogeneous with a large range of RBC velocities and a high capillary transit time heterogeneity (Jespersen and Østergaard, 2012).
This is also reflected in the number of available pathways through the capillary bed and the frequencies with which these are chosen. Five exemplary RBC pathways through the cortical microvasculature are illustrated in Figure 3D. We recently showed that for each capillary starting point there are on average 8 different RBC pathways leading from DA to AV. However, for more than 50% of all capillary starting points there is a preferential path which is chosen with a frequency > 50% (Schmid et al., 2017). Furthermore, our results revealed that the capillary starting point and the capillary end point are strongly correlated (Figure 3C) and hence, the RBC tend to move "in-plane" through the capillary bed (Schmid et al., 2017). It seems likely that the capillary bed is designed to encourage the in-plane (i.e. parallel to the surface) motion of RBCs.
All in all, even though the structure of the capillary bed is commonly described as being homogeneous its flow field is highly heterogeneous. Further investigations are necessary to thoroughly explain the observed characteristics.
Similarly to the pial and penetrating vessels, occlusion experiments have been performed to assess the overall robustness of the capillary bed in the distribution of flow (Figure 3F; (Nishimura et al., 2007; Shih et al., 2013)). Nishimura et al. (2007) and Shih et al. (2013) showed that the impact of a microvessel occlusion is minimal and that the RBC flux recovered to 45% of its baseline value by three branches downstream of the occlusion. The robustness of the capillary bed can be explained by its mesh-like structure, which is beneficial for an efficient redistribution of flow. Furthermore, Guibert et al. (2012) show that 63% of all capillaries are fed by more than one DA and hence a redundancy towards DA occlusion persists as well. Interestingly, the robustness of the capillary bed towards DA occlusion increases with depth (Figure 3G; Guibert et al. (2012)). It has also been suggested that capillary bed density might correlate with neuronal functional units. For the barrel cortex no such correlation was observed (Blinder et al., 2013). Similarly to the penetrating vessels, the results of Keller et al. (2011) and Adams et al. (2014) diverge for the blobs in the visual cortex, and only Keller et al. (2011) noted a slightly increased vessel density within the blobs.

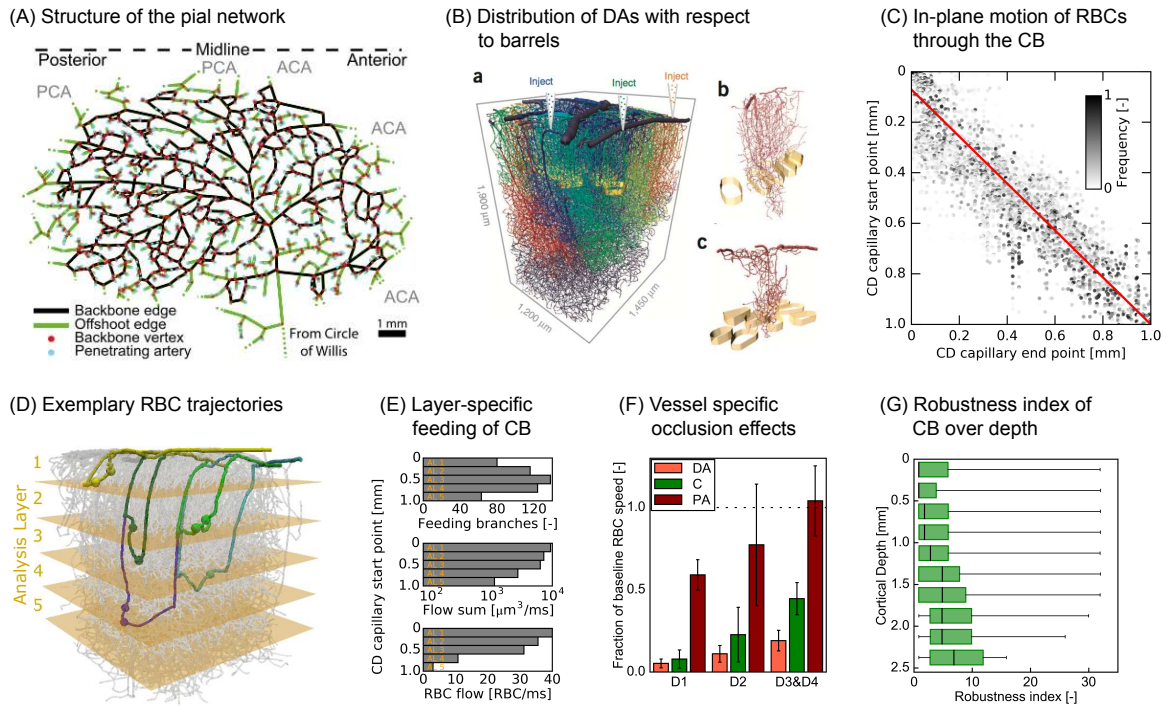


Figure 3 Topological characteristics of the cerebral vasculature. (A) Exemplary pial network. The backbone of the pial network is highlighted in black (Figure from Blinder et al. (2010)). (B) Feeding regions of descending arteries (DAs) and their distribution with respect to whisker barrels ("golden bands"). The colors indicate feeding regions for different DAs. (Figure from Blinder et al. (2013). Reprinted by permission from Macmillan Publishers Ltd: Nature Neuroscience, 2013). (C) Cortical depth (CD) of capillary start and capillary end points to illustrate the in-plane motion of RBCs in the capillary bed (CB) (Figure from Schmid et al. (2017)). (D) Exemplary RBC trajectories for different depths of capillary starting points (Figure from Schmid et al. (2017)). (E) Layer-specific feeding characteristics of the capillary bed (CB) (Figure from Schmid et al. (2017)). (F) Impact of occlusion for different vessel types (DA: descending arteries, C: capillaries, PA: pial arteries). The impact is measured based on the fractional RBC speed in vessel segments downstream the site of occlusion (D1: one segment downstream, D2: two segments downstream, D3&D4: three and four segments downstream) (Figure adapted from: Nishimura et al. (2007)). (G) Robustness index of the capillary bed (CB) for different cortical depths. The robustness index is defined as the number of descending arteries feeding a capillary segment (Figure adapted from: Guibert et al. (2012)).

## 6 Flow regulation

In the previous section we described static characteristics of the cerebral vasculature, yet the vasculature is constantly adapting to the metabolic needs of the parenchyma. The resulting hemodynamic changes are the basis of a multitude of imaging techniques. Understanding the vascular topology goes hand in hand with understanding the vascular response to neuronal activation. Hence, in the following we summarize the current knowledge on vascular regulation mechanisms. We begin by describing the candidate locations for regulation and the contractile cells in their surroundings. Subsequently, we comment on spatio-temporal and layer-specific dynamics of regulation. The neurovascular signaling pathways are not addressed in this manuscript. A good overview is given in the reviews by Iadecola and Nedergaard (2007), Attwell et al. (2010) and Hillman (2014).

### 6.1 Contractile cells of the cerebral vasculature

Two cell types have been reported to modulate vascular diameter in vivo: smooth muscle cells and pericytes. While the involvement of smooth muscle cells in neurovascular coupling is well established, the contractility of pericytes in vivo has been shown only recently and their role in neurovascular coupling is a matter of ongoing debate (Attwell et al., 2010; Attwell et al., 2015; Fernandez-Klett et al., 2010; Fernández-Klett and Priller, 2015; Hall et al., 2014; Hill et al., 2015; Hillman, 2014; Itoh and Suzuki, 2012).
Arterial smooth muscle cells (SMCs) are tightly wrapped around arteries and hence perfectly positioned to control vessel diameters (Figure 4A). Pericytes differ significantly in their shape and in the expression of $\alpha$ smooth muscle actin ($\alpha$-SMA). While in the smooth muscle cells around DAs $\alpha$-SMA is omnipresent in pericytes it only persists close to the DA (Figure 4A; (Attwell et al., 2015; Hartmann et al., 2015; Hill et al., 2015)). However, it remains unclear if $\alpha$-SMA is a prerequisite for the contractility of pericytes or if other, as yet unknown mechanisms for altering the diameter of capillaries exist (Fernández-Klett and Priller, 2015).

### 6.2 Vascular response of different vessel types to neuronal activation

The overall hemodynamic response to neuronal activation results from an interplay of different vascular responses (Hillman, 2014). In this subsection, we discuss the response and spatio-temporal dynamics of individual vessel types, namely: (1) pial and descending arteries, (2) pre-capillary arteries and capillaries, and (3) venules and veins. Table 3 summarizes the key characteristics of the vascular response of different vessel types to brief stimulation (< 5 s).
In general the location where the vascular response is initiated depends on the cortical area under investigation and the type of stimulus applied. For the rat primary somatosensory cortex and the stimulation of the forepaw the prevailing view is that the response starts as deep as 0.6-0.9 mm in the cortex and spreads towards the surface with a propagation speed of ~0.9 mm/s (Tian et al., 2010; Uhlirova et al., 2016b). The vasculature itself may be responsible for the propagation of the dilatory signal (Chen et al., 2011; Chen et al., 2014; Hillman, 2014; Iadecola et al., 1997; Uhlirova et al., 2016b), but it remains unclear if vasodilation is triggered at a specific vessel type only.
Lindvere et al. (2013) were the first to monitor diameter changes simultaneously in a microvascular network spanning 0.5 x 0.5 x 0.6 mm. They show that even along individual vessels the response is heterogeneous, which adds to the complexity of the vascular response. In order to analyze changes in the whole network, they introduce the concept of early and late responding vessels. While they observe an upward propagation of early dilations and late constrictions, the early constrictions and late dilations spread with increasing depth.
The stimulus length as well as the used anesthesia can play a role in the vascular response. Drew et al. (2011) showed that the longer the stimulus the larger the vasodilation until a plateau dilation is reached. The effects of anesthesia have been investigated by Lyons et al. (2016) and Masamoto et al. (2009). Their works show that the level of anesthesia affects the increase in cerebral blood flow as well as the tissue oxygen partial pressure. Furthermore, one has to bear in mind that baseline fluctuations in diameter persist, which for the pial vessels have the same order of magnitude as functional diameter changes (Drew et al.,

2011). All in all, the spatio-temporal dynamics of neurovascular coupling are highly complex and difficult to elucidate, partly due to their mutual interdependence.

| Vessel type | Maximum dilation | Average peak dilation | Onset time | Time to peak |
|---|---|---|---|---|
| Pial arteries | 31.6 ± 4.1 % | 11.0 ± 3.5 % | 1.0 ± 0.1 s | 2.9 ± 1.1 s |
| Descending arteries | 31.0 ± 5.0 % | 9.7 ± 2.2% | 0.8 ± 0.2 s | 2.4 ± 0.4 s |
| Capillaries* | 40% | 13.3 ± 2.0 % | 1.7 ± 1.0 s | 2.8 s |

Table 3: Key characteristics of the vascular response of different vessel types. The given values are the average and the standard deviation of all values found in literature for short sensory stimulation (< 5 s). Capillaries*: Data on in vivo capillary dilation is very sparse. Thus, we also considered the measurements by Hall et al. (2014) although the stimulus duration is 15s. Furthermore, for capillaries it was not always clear if the given values are for active or passive dilation. Maximum dilation: maximum dilation that has been measured in individual vessels. Average peak dilation: average over all measured dilations. Onset time: time after start of stimulus until dilation is initiated. Time to peak: time after begin of the stimulus until the maximum dilation is reached. Reference literature: Pial arteries: (Devor et al., 2008; Devor et al., 2007; Drew et al., 2011; Hillman et al., 2007; Sekiguchi et al., 2014; Tian et al., 2010; Uhlirova et al., 2016b). Descending arteries: (Sekiguchi et al., 2014; Tian et al., 2010; Uhlirova et al., 2016b). Capillaries: (Hall et al., 2014; Tian et al., 2010).

*Pial and descending arteries:*

As mentioned in Section 5.1 the pial network is responsible for a robust supply of blood to different tissue regions. Furthermore, it has been hypothesized that it redistributes blood during neuronal activation (Devor et al., 2007; Shih et al., 2015).

As the pial vasculature is comparably easy to access, many works have recorded vascular changes at the pial level (Chen et al., 2014; Devor et al., 2008; Devor et al., 2007; Drew et al., 2011; Hillman et al., 2007; Ngai et al., 1988; Ngai and Winn, 2002; Sekiguchi et al., 2014; Tian et al., 2010; Uhlirova et al., 2016b). Despite differences in methodology and/or species, all studies agree that multiple pial arteries alter their diameter in response to neuronal activation.

The largest changes are located close to the center of activation (CoA), and the amplitude of the relative diameter change decreases with the distance from the CoA (Figure 4B). Positive diameter changes have been observed up to 3 mm away from the CoA; however, for distances > 2 mm the vascular response is predominantly negative (i.e. more constrictions than dilations (Devor et al., 2008; Devor et al., 2007)).

For many pial arteries there is a period of constriction after stimulus cessation, for reasons not currently understood (Figure 4B). However, the amplitude of constriction is significantly smaller than that for dilation (Devor et al., 2007; Drew et al., 2011; Hillman et al., 2007; Uhlirova et al., 2016b).

The DAs feed the capillary bed with blood from the cortical surface. As they pose the "bottleneck of perfusion" (Nishimura et al., 2007) it seems likely that they are also ideally placed for a localized increase in blood flow, and there is a large body of evidence showing the dilation of DAs during activation (Attwell et al., 2010; Hall et al., 2014; Hillman, 2014; Iadecola and Nedergaard, 2007; Lindvere et al., 2013; Tian et al., 2010; Uhlirova et al., 2016b). Based on the results of Hall et al. (2014) ~50% of the monitored DAs responded to

neuronal activation. However, it remains unknown how those are distributed with respect to the CoA.
Recent studies have reported that the dilation of DAs is initiated deep in the cortex (measurements up to 0.9 mm) and propagates towards the cortical surface (Figure 4C, (Lindvere et al., 2013; Tian et al., 2010; Uhlirova et al., 2016b)).
Uhlirova et al. (2016b) showed that approximately 50% of all responding DAs experience a post-stimulus constriction phase. As for the pial vessels, the amplitude of constriction is significantly lower than for dilation.
It is still debated if the amplitude of dilation is a function of cortical depth, and results concerning this matter have been diverging (Figure 4C) (Lindvere et al., 2013; Sekiguchi et al., 2014; Tian et al., 2010; Uhlirova et al., 2016b). Even though it is well known that DAs dilate during activation the detailed patterns of their response still have to be elucidated.
Although lacking the resolution to distinguish between changes originating from pial and descending arteries, a range of MRI techniques have also reported substantial increases in arterial blood volume upon stimulation, generally consistent with the diameter measurements discussed above (Ho et al., 2011; Kim et al., 2007; Kim and Kim, 2010).
A further interesting aspect of the vascular response is the return to baseline. However, this aspect is less studied than the onset of dilation and strongly depends on the duration of stimuli. It has been hypothesized that there is a distinct regulation mechanism, which is responsible for the decay phase (Chen et al., 2011). Approximately 4 s after stimulus cessation, the pial vessels reach their baseline diameter at which they remain or continue to constrict (Devor et al., 2008; Sekiguchi et al., 2014; Tian et al., 2010). The return to baseline of pial vessels does not depend on the distance to the neuronal CoA (Devor et al., 2007).

*Pre-capillaries and capillaries:*
Over the past years more evidence for the relevance of capillaries for neurovascular coupling has emerged (Hall et al., 2014; Tian et al., 2010). As capillaries are the vessels most proximal to the largest part of tissue it seems plausible that they may play a role in the up-regulation of flow, oxygen and energy substrate delivery. However, there is relatively little data available, and it is challenging to differentiate between effects resulting from arteriole and capillary dilation in vivo. In the following, we comment on direct and indirect evidence that supports the hypothesis of an active involvement of capillaries in neurovascular coupling.
A crucial argument for active capillary dilation has been provided by Hall et al. (2014). They demonstrate that capillaries dilate on average 1.4 s prior to arterioles, which eliminates the possibility of a purely passive response of capillaries. Additionally, they report that capillaries are more likely to respond in the vicinity of pericytes (50% vs. 22% response frequency) and that the frequency of responding capillaries decreases with branching order. This observation is in line with a decrease in $\alpha$-SMA for pericytes located at higher branching orders (Attwell et al., 2015; Hartmann et al., 2015; Hill et al., 2015). Similarly to DAs, capillaries located deep in the cortex dilate earlier than the ones close to the cortical surface (Tian et al., 2010). Whether or not the resistance at the level of small vessels is regulated by pericytes or smooth muscle cells remains a matter of ongoing debate (Attwell et al., 2015; Hartmann et al., 2015; Hill et al., 2015), which may be caused in part by different definitions of pericytes and/or capillaries.
However, the observations by Hall et al. (2014) are in contrast to the results of Tian et al. (2010) who state that the dilation spreads from the DAs to the capillary bed. The work by

Chen et al. (2011) supports an onset of vasodilation at the capillary level, because they reported an increase in total hemoglobin in the parenchyma prior to the increase in the arterioles. The origin of those differences is not yet clear.
A number of studies provide further indirect evidence for an active regulation mechanism at the capillary level leading to a homogenization of flow (Gutiérrez-Jiménez et al., 2016; Lee et al., 2014; Lee et al., 2015; Stefanovic et al., 2008). Lee et al. (2015) measured the RBC flux in ~200 capillaries simultaneously, during baseline and activation, and showed that the standard deviation of RBC flux decreased 2 s prior to the increase in the mean. This agrees with the observations of Stefanovic et al. (2008) and Gutiérrez-Jiménez et al. (2016), who reported that low baseline flux capillaries experience a larger response to stimulation. Furthermore during activation, the capillary transit time heterogeneity is reduced (Gutiérrez-Jiménez et al., 2016). The altered RBC velocities and the homogenization of flow following neuronal activation may also partly result from a pO2-dependent increase in RBC flexibility (Wei et al., 2016).
It should also be kept in mind that capillary dilation can be an effective means to alter the distribution of RBCs (Schmid et al., 2015), and that flow homogenization during neural activation may play an important role in oxygen delivery (Barrett and Suresh, 2013; Jespersen and Østergaard, 2012; Vazquez et al., 2008).

*Venules and Veins*
No active dilation of venules and veins has been reported; however, there are conflicting reports about the presence and/or significance of passive dilation of venules and veins. For example, direct optical measurements of venous diameter have shown either no increase (Hillman et al., 2007) or very small increases (Drew et al., 2011), whereas MRI-based approaches have reported considerable increases in venous blood volume (Chen and Pike, 2009; Chen and Pike, 2010). However, using a biophysical model, Barrett et al. (2012) demonstrated that these discrepancies could be explained by differences in stimulation length (typically short in optical imaging experiments, but long in MRI experiments) and the fact that even relatively small changes in capillary and/or venous diameters can lead to large changes in venous CBV. Taken alongside the experimental evidence, this result suggests that, for brief stimulation, dilation of arteries and arterioles contributes the majority of blood volume increases; however, dilation of post-arteriolar vessels is relevant during longer stimulation (>10 s).

### 6.3 Layer-specific regulation

In the cortex the distribution of neurons and consequently the metabolic needs vary over depth. We have already briefly commented on the propagation of vasodilation over depth. Yet the question remains whether those differences are also an indication for layer-specific regulation mechanisms. Here, we summarize the available evidence for the existence of layer-specific regulation, and we discuss why layer-specific regulation seems plausible with respect to the flow field from a fluid dynamics point of view.
Direct evidence for layer-specific regulation mechanisms is still relatively sparse. To investigate whether the response to stimulation varies over depth, Gutiérrez-Jiménez et al. (2016) measured RBC velocity, RBC flux and capillary transit time with two-photon

microscopy. A range of high resolution MRI studies have also observed layer-dependent changes in CBF and/or CBV (Goense et al., 2012; Hirano et al., 2011; Ho et al., 2011; Huber et al., 2015; Huber et al., 2016; Kim and Kim, 2010, 2011; Zhao et al., 2006). Both approaches agree that the hemodynamic response varies over depth, which points towards layer-specific regulation mechanisms. However, these differences could also result passively from laminar variations in vascular topology.
In the cerebral microvasculature depth-dependent flow and pressure characteristics persist (Figure 4D) and provide further evidence why layer-specific regulation might be beneficial (Gutiérrez-Jiménez et al., 2016; Kleinfeld et al., 1998; Lee et al., 2014; Schmid et al., 2017). We recently analyzed the pressure drop along the pathway of individual RBCs and showed that the deeper the RBC enters the capillary bed the larger the pressure drop in the DA and the smaller in the capillary bed (Figure 4E, Schmid et al. (2017)). The pressure drop has a strong impact on the increase in flow rate resulting from dilation. Hence, our results support the hypothesis that layer specific regulation could be advantageous.
Additionally, various experimental as well as numerical works observe that the RBC velocity decreases over depth and consequently the capillary transit time increases (Figure 4D) (Gutiérrez-Jiménez et al., 2016; Kleinfeld et al., 1998; Lee et al., 2014; Schmid et al., 2017). These factors strongly impact the amount of oxygen discharged from RBCs and therefore it seems likely that the oxygen discharge also varies over depth (Section 7.3).

### 6.4 Dimension of the area affected by neuronal activation

In order to discuss the dimensions of the area affected by neuronal activation it is important to distinguish between (1) the area in which the vasculature responds to stimulation and (2) the area that is affected by the altered vessel diameters.
Relatively little is known about the precise spatial pattern of the vascular response. At the pial level diameter changes have been recorded up to 3 mm apart from the CoA (Devor et al., 2008; Devor et al., 2007). Based on the concept of retrograde propagation it seems likely that those vessels are located upstream of the neuronal CoA (Erinjeri and Woolsey, 2002; Iadecola et al., 1997). However, the results from Chen et al. (2011) suggest that the vasodilation spreads “spatially outwards” and is independent of the flow direction. Even if the precise pattern of vessel recruitment is not yet fully understood, a selective recruitment of vessels seems likely (Erinjeri and Woolsey, 2002; Hillman, 2014). A better knowledge of the signaling pathways and measurements of diameter changes with high temporal and spatial resolution are necessary to advance our understanding of the vascular response patterns.
The dimension of the area that is affected by the altered vessel diameter strongly depends on the location of the vessel along the vascular pathway: the further upstream the larger the area affected. Illustrative proof is given in the numerical work by Reichold et al. (2009). They showed that if the site of dilation along the DA is close to the cortical surface its area of influence is larger than if it is located further downstream.
To investigate this in vivo is difficult, because changes in a large volume have to be monitored simultaneously. Frequently, techniques which measure 2D projections of the flow field are applied. For example, Dunn et al. (2005) use multi-wavelength reflectance imaging to estimate the spatial extent of hemodynamic changes during functional

activation. They show that the surface area where a change in total hemoglobin is noted differs for forepaw and whisker stimulation: ~2.0mm$^2$ and ~1.6mm$^2$, respectively.

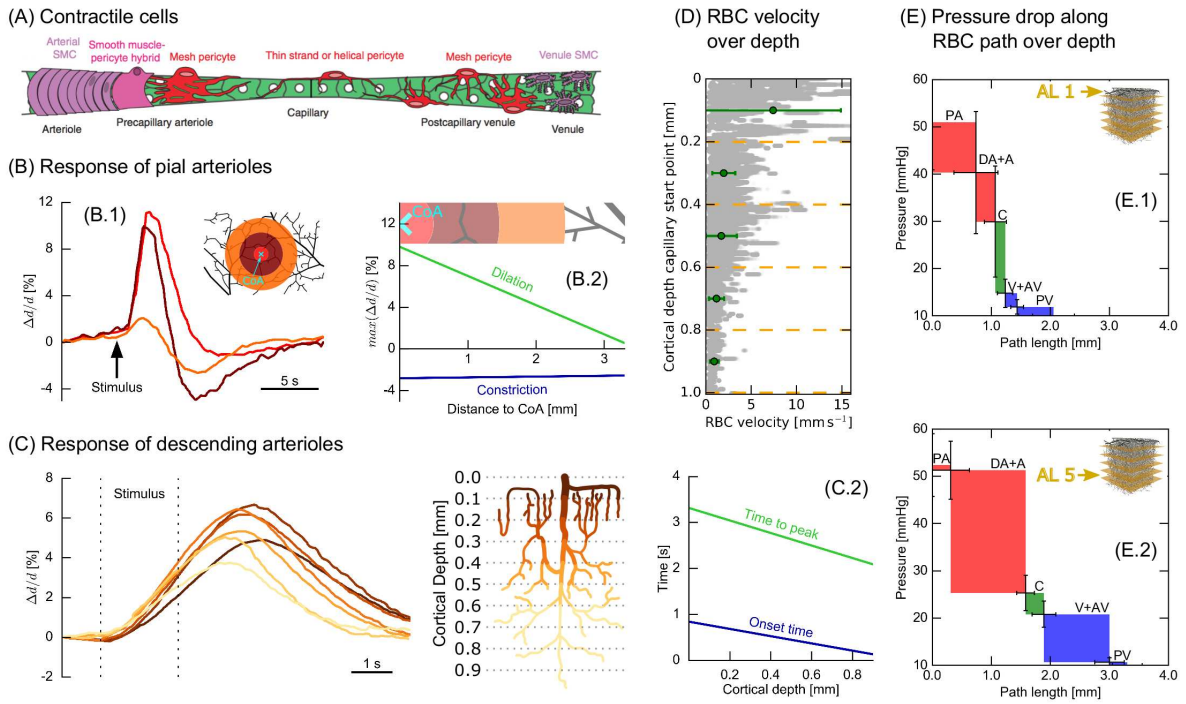


Figure 4 Vascular response to neuronal activation and flow characteristics. (A) Schematic representation of smooth muscle cell and pericytes in the cerebral vasculature (Figure from: Hartmann et al. (2015)). (B) B.1: Response of pial arteries to stimulation as a function of time for different distances to the neuronal center of activation (CoA). Distances: red: 0-0.5 mm, dark red: 0.5-1.5 mm, orange: 1.5-2.5 mm. B.2: Maximum dilation/constriction for pial arteries as a function of the distance to the CoA (Figure adapted from: Devor et al. (2007). Pial vasculature in insert adapted from: Schaffer et al. (2006)). (C) C.1: Response of descending arteries to stimulation as a function of time for different depths. C.2: Onset time and time to peak for descending arteries as a function of cortical depth (Figure adapted from: Uhlirova et al. (2016b). Schematic drawing of a descending artery adapted from: Duvernoy et al. (1981)). (D) RBC velocity in the capillary bed over depth (Figure from: Schmid et al. (2017)). (E) Pressure drop along RBC trajectories for analysis layer 1 (AL 1: 0 – 200 µm cortical depth) and analysis layer 5 (AL 5: 800 – 1000 µm cortical depth) for different vessel types. The analysis layers are 200 µm thick slices for which different flow characteristics are analyzed. (Figure from: Schmid et al. (2017)).

## 7 Oxygenation

Impairments to cerebral blood flow on the order of a few minutes are sufficient to cause irreversible hypoxic ischemic injury (Jones et al., 1981; Moskowitz et al., 2010). Therefore supplying oxygen, along with metabolic substrates, is the most critical role of the brain vasculature. In this section we provide a brief overview of cerebral oxygenation, especially as it relates to laminar fMRI.

### 7.1 Baseline oxygenation

In the traditional view of oxygenation in the brain, arteries provide constant supply of oxygenated blood, capillaries are the site of oxygen delivery, and veins drain deoxygenated blood. However, evidence has emerged that challenges this concept. For example, several studies reported that blood in cortical arteries and particularly arterioles is not completely

oxygenated (Devor et al., 2011; Lyons et al., 2016; Sakadžić et al., 2014; Vazquez et al., 2010; Vovenko, 1999; Yaseen et al., 2011). In addition, direct measurements (Sakadžić et al., 2014) and combined morphological and functional data (Kasischke et al., 2011) suggest that arterioles supply a significant fraction of the total oxygen to the tissue under baseline conditions. Furthermore, there is conflicting evidence about the presence and/or significance of oxygen gradients surrounding venules and veins (Devor et al., 2011; Vazquez et al., 2010; Vovenko, 1999), and oxygen shunts from arterial to venous vessels were also directly observed *in vivo* (Lecoq et al., 2011), consistent with a number of studies that have reported increases in venous pO2 (Sakadžić et al., 2014; Vazquez et al., 2010; Vovenko, 1999; Yaseen et al., 2011). Nonetheless, in rodents, pO2 values in arteries and arterioles typically fall between 60 and 110 mmHg, values in capillaries vary from 20-60 mmHg, and values in veins and venules range from 30 to 60 mmHg (Lyons et al., 2016; Parpaleix et al., 2013; Sakadžić et al., 2014; Vazquez et al., 2010; Vovenko, 1999; Yaseen et al., 2011).
It is important to note that differences in oxygenation between awake and anaesthetized animals have been reported, and although overall capillary pO2 appeared similar in the mouse olfactory bulb and somatosensory cortex, this may not be true for all regions, particularly since measurements of RBC flux and linear density did differ between the two regions (Lyons et al., 2016). In addition, since experimental and modeling evidence suggests the existence of erythrocyte-associated transients (EATs; (Golub and Pittman, 2005; Hellums, 1977; Lecoq et al., 2011; Lücker et al., 2015; Parpaleix et al., 2013)), there may be substantial discrepancies between true hemoglobin saturation and that estimated based on average blood pO2 (Lyons et al., 2016). The opposite case is also relevant, since oxygen saturation is often measured using techniques like intrinsic imaging of optical signals (Dunn et al., 2003) or photoacoustic tomography (PAM; (Yao et al., 2015)) and the measured saturation may therefore overestimate mean blood pO2.

### 7.2 Activation-induced changes in oxygenation

In response to activation, dynamic pO2 increases have been reported in all vessel types (Lecoq et al., 2011; Parpaleix et al., 2013; Vazquez et al., 2010; Yaseen et al., 2011). Prior to the main positive response, a brief, relatively small decrease in pO2 has also been observed in capillaries and parenchymal regions close to capillaries (Lecoq et al., 2011; Parpaleix et al., 2013; Wei et al., 2016). This early response, often called the 'initial dip', has been controversial in the optical imaging and fMRI communities due to conflicting reports (Buxton, 2001; Hu and Yacoub, 2012). Some reports suggest that the initial dip may be more spatially specific than the subsequent increase in signal (Vazquez et al., 2010).
There is also some uncertainty regarding the magnitude and importance of pO2 increases in the tissue following activation. Many studies have observed robust increases in tissue pO2 (Lecoq et al., 2011; Parpaleix et al., 2013; Thompson et al., 2003; Vazquez et al., 2010) and, using a drug that pre-dilated arteries to prevent further activation-induced CBF increases, Masamoto et al. (2008) showed that these tissue pO2 increases under normal conditions occurred in spite of increased oxygen demand in the tissue. In contrast, Devor et al. (2011) reported that, during sustained stimulation, there was no pO2 increase in regions of the tissue with low baseline pO2. The authors proposed that activation-induced increases in CBF may occur to prevent dangerous levels of hypoxia in these regions; however, it is unclear

whether changes in CBF without any increase in CMRO2 would lead to pO2 increases in these regions, or if they were simply too far from the vasculature to be noticeably affected.

### 7.3 Laminar oxygenation

To the best of our knowledge, there are only very few studies that have reported direct laminar measurements of oxygenation in the brain, partly because of the technical difficulties in obtaining such data. For example, electrode measurements are invasive, especially at depth, and current optical approaches have limited depth penetration (Lecoq et al., 2011; Sakadžić et al., 2010). Furthermore, the studies that do exist are somewhat contradictory. Using two-photon phosphorescence lifetime microscopy (2PLM) in alpha-chloralose anesthetized rats, Devor et al. (2011) reported a substantial decrease in estimates of arterial oxygenation from the surface to ~200µm into the cortex; however, Lyons et al. (2016), using the same technique in awake mice, did not observe any significant depth-dependence in arterial or venous pO2 in the upper 400µm of the cortex. Devor et al. (2011) also observed noticeable decreases in tissue pO2 in the upper ~300µm of the cortex, which is consistent with previous measurements using oxygen sensitive microelectrodes (Masamoto et al., 2003). Masamoto et al. (2003) were able to measure throughout the cortical grey matter, deeper into the cortex. All three somatosensory regions considered showed a substantial pO2 decrease from the surface to layer II, but the forelimb and hindlimb areas showed further variation, peaking around layer V, while the trunk region remained fairly constant. Note that in all of these studies, pO2 in the upper cortical layers may have been influenced by the surgical preparation, including removal of the skull. Although their measurement technique (constant potential amperometry) was not able to generate measurements of *baseline* pO2, Li et al. (2011) reported simultaneous, high temporal resolution measurements of *changes* of tissue pO2 at multiple cortical depths in response to electrical stimulation of the rat whisker pad. The authors observed a generally biphasic response, whereby the pO2 initially decreased, most strongly in layer IV, and subsequently increased, with the largest increases occurring in the upper cortical layers. Applying a nitric oxide synthase inhibitor to reduce activation-induced CBF increases made the pO2 responses more negative at all depths. While this study offers an interesting initial view into laminar differences in oxygenation, further studies, ideally using complementary techniques such as 2PLM or PAM, are needed to investigate these complex changes.

## 8 Relevance of vasculature for (laminar) fMRI

The vasculature is relevant for a number of MRI techniques, including the diffusion and perfusion weighted imaging approaches commonly used in clinical diagnosis and treatment of neuropathologies such as tumors, stroke, and transient ischemic attack (Fink et al., 2015; Souillard-Scemama et al., 2015). However, in this review we focus on the relevance of the vasculature for BOLD-fMRI.

Although the details of the underlying physics of the fMRI signal are beyond the scope of this review, the equation from Buxton (2013) listed below (Equation 1) serves to summarize the ways in which the vasculature can influence the BOLD signal. (Readers interested in the derivation of this equation or a more rigorous introduction to the relevant physics are highly recommended to consult Buxton (2013)). We focus here on the more commonly used

gradient echo (GE) technique, but note that there are important differences between gradient echo and spin echo (SE) sequences. For example, GE sequences are typically more sensitive to larger vessels, particularly veins, than SE (Boxerman et al., 1995b; Menon, 2012).
Briefly, the BOLD signal change normalized to baseline, $\Delta S/S_0$, can be described such that

$$\Delta \boldsymbol{S/S_0} = \boldsymbol{k \cdot TE \cdot V_0 \cdot D_0^{\beta} \cdot (1 - v \cdot d^{\beta})}, \quad (1)$$

where $V_0$ is the baseline blood volume, $D_0$ is the baseline concentration of deoxyhemoglobin, $v$ and $d$ are the dynamic blood volume and deoxyhemoglobin concentration normalized to their respective baselines, $k$ is a constant related to the MRI field strength, $TE$ is the echo time, and $\beta$ is a constant describing the effect of deoxyhemoglobin on the relaxation rate. While the blood volume terms are relatively self-explanatory, it is worth emphasizing that local deoxyhemoglobin concentration reflects the balance of two competing processes: oxygen delivery (via CBF), and oxygen consumption (CMRO2). Since CBF generally increases more than CMRO2 during activity (Fox and Raichle, 1986), the concentration of deoxyhemoglobin decreases, and the BOLD signal increases (Ogawa et al., 1990).
Although fMRI has primarily been used to localize neuronal activity, there is an increasing desire to use it as a quantitative tool to measure CMRO2 changes (Buxton, 2013). Earlier studies suggested that CMRO2 changes primarily reflected energy use associated with neuronal signaling (Attwell and Laughlin, 2001). As such, a longstanding aim of the neuroimaging community has been to 'unmix' or 'deconvolve' the vascular component from the measured fMRI response, in order to isolate the metabolic contribution to the signal. However, a more recent hypothesis proposes that different types of neuronal activity, e.g. excitatory vs inhibitory signaling, may have distinct effects on changes in CBF, CMRO2, and electrical activity (Buxton et al., 2014; Uhlirova et al., 2016a). In the following sections, we provide an overview of the ways in which the vasculature influences the BOLD response, including those aspects particularly relevant to laminar fMRI.

### 8.1 Baseline blood volume and deoxyhemoglobin concentration

As shown in Equation (1), the baseline values of CBV and dHb concentration act to scale the magnitude of the BOLD signal change for a given change in CBV and dHb. This means that, depending on the baseline values of CBV and dHb, different changes in CBV and dHb could result in the same BOLD signal change and, inversely, that different BOLD signal changes could result from the same changes in CBV and dHb. Given that CBV and pO2 (likely reflecting differences in dHb) vary between different cortical regions, and indeed layers (Section 4 and Section 7), this effect is important to consider when comparing BOLD responses from different locations.
The baseline value of dHb concentration also imposes a theoretical limit on the maximum achievable BOLD increase, since dHb concentration can only decrease from its baseline value to zero, and not below. In addition, it is also important to note that, despite previous assumptions to the contrary (Davis et al., 1998; Dunn et al., 2005; Hoge et al., 1999; Mayhew et al., 2000), capillaries and even arterioles contain a non-negligible amount of deoxyhemoglobin (Section 7; (Lyons et al., 2016; Sakadžić et al., 2014; Yaseen et al., 2011)). Evidence from a recent modeling study suggests that assuming arterial hemoglobin is

completely saturated can lead to errors when estimating CMRO2 (Barrett and Suresh, 2015).

### 8.2 Activation-induced changes in blood volume and deoxyhemoglobin

Deoxyhemoglobin concentration reflects the dynamic balance of changes in CBF and CMRO2, so it is important to consider the spatiotemporal interplay of these two processes. In terms of CBF, some authors suggest that the spacing between penetrating vessels represents a limit on the minimal achievable point spread function (PSF) of BOLD-fMRI measurements (Turner, 2016; Uludağ and Blinder, 2017). This would be concerning for the utility of high resolution and laminar fMRI, particularly considering that combined anatomical and functional data from the mouse barrel cortex showed that the location of descending arteries and ascending veins did not correlate with whisker barrel regions (Blinder et al., 2013). In addition, diameter changes in descending arteries in the cat visual cortex were recently shown to be less selective for stimulus orientation than calcium signals in the neurons surrounding them (O'Herron et al., 2016). However, the conclusion that penetrating vessel geometry limits the PSF of BOLD-fMRI may be premature, for two reasons.

First, as discussed in Section 6, flow regulation may also occur at sites downstream of descending arteries, such as pre-capillary arterioles, capillaries, and perhaps even via red blood cells themselves (Wei et al., 2016). This would allow CBF changes to be regulated over a much finer spatial scale than the territory of a single descending artery.

Secondly, changes in CBF represent only one of the effects leading to the changes in dHb that drive the BOLD signal; changes in CMRO2 also play a vital role. Therefore, even if CBF increases occur over a larger or different area than the region of neuronal activity, or with different kinetics, modeling approaches that make use of multimodal data may be able to decouple the effects of layer-dependent changes in CBF and CMRO2 on dHb (Gagnon et al., 2015; Heinzle et al., 2016; Markuerkiaga et al., 2016). Any differences between the CBF and CMRO2 response may also help to infer the nature of the underlying neural activity (Uhlirova et al., 2016a).

The influence of CBV changes on the BOLD signal are complex. Part of this may be related to difficulties in distinguishing between direct effects of volume changes on the signal, and indirect effects that relate to volume changes. As per Equation (1), early simulations and experiments showed that pure increases in CBV tend to reduce the BOLD signal change (Boxerman et al., 1995a; Ogawa et al., 1993; Yablonskiy and Haacke, 1994). However, in practice, an increase in arterial blood volume may somewhat increase the signal, by exchanging volume with the extravascular fluid, which has a weaker signal (Buxton, 2013). Furthermore, increases in venous blood volume would also typically increase the concentration of dHb in a voxel, leading to reduced BOLD signal.

Several recent studies, using elegant approaches to produce spatially confined responses, have observed that activation-induced changes in CBV appeared more specific and localized to neuronal activity than BOLD responses (Moon et al., 2013; Poplawsky et al., 2015). While these are interesting results, it is important to note that changes in CBV are a purely vascular response, and so do not contain any information about the changes in CMRO2 thought to derive more directly from neuronal activity. Nonetheless, combining high resolution CBV imaging with CBF and BOLD measurements into a detailed biophysical model

would be a particularly powerful approach for probing neuronal activity non-invasively (Uhlirova et al., 2016a).

### 8.3 Direct MR effects

The vascular structure itself can also have a direct influence of on the BOLD signal. Using detailed reconstructions of the microvasculature coupled with high resolution functional measurements, Gagnon et al. (2015) recently developed a 'bottom up' model of the BOLD signal which predicted that activation-induced signal changes would vary by up to 40%, depending on the orientation of the cortex to the scanner's primary magnetic field. The effect was present only when using gradient echo, rather than spin echo, pulse sequences, and derives from the fact that the orientation of larger veins is not isotropic, since they are predominantly aligned either in parallel with or perpendicular to the cortical surface (Gagnon et al., 2015). This orientation dependence is particularly relevant for data from human and primate brains, since the folding pattern of gyri and sulci produces a significant variation in local surface orientation (Cohen-Adad et al., 2012), which is not present in lissencephalic animals. Although the model developed by Gagnon et al. (2015) used the vascular structure from mice, rather than primates, and functional data from rats, predictions from their model agreed very well with human data. However, given that the imaging voxel size was 3.4x3.4x6mm, it remains to be seen whether such orientation dependence exists through the cortex, at the higher spatial resolution typical for laminar fMRI.

## 9 Outlook

We have tried to compile the current status of research on the cortical vascular system in the present review. As mentioned, the vascular system is at the basis for many important topics in neuroscience, both in health and disease. Many aspects remain insufficiently understood. First and foremost, the human cortical vascular system has not been studied quantitatively, and many of our current concepts rely on rodent data. It is therefore important that novel technical approaches emerge that allow vascular labelling and imaging of human post-mortem tissue. This will directly lead us to addressing relevant questions regarding the involvement of (micro-)vascular network alterations in neurodegenerative diseases. Another important future research direction concerns the size of the reconstructed networks. Much of what we know today relies on relatively small (few cubic millimeters) networks. It is desirable that whole brain vascular system reconstructions become available, which seems feasible at least in the mouse. This would significantly reduce the problem of the boundary conditions for modeling blood flow dynamics. Furthermore, blood flow dynamics must eventually be studied in vivo, and methods are needed that can cover entire microvascular networks with sufficient spatial and temporal resolution to capture dynamics at the single red blood cell level.

## 10 Acknowledgements

Funding for this work was provided by the University and ETH Zurich and the Swiss National Science Foundation Grant No. 140660. BW is a member of the Clinical Research Priority Program of the University of Zurich on Molecular Imaging. MB is supported by the Forschungskredit of the University of Zurich.

**References**

Adams, D.L., Piserchia, V., Economides, J.R., Horton, J.C., 2014. Vascular supply of the cerebral cortex is specialized for cell layers but not columns. Cerebral Cortex, bhu221.

Armulik, A., Genove, G., Betsholtz, C., 2011. Pericytes: developmental, physiological, and pathological perspectives, problems, and promises. Dev Cell 21, 193-215.

Attwell, D., Buchan, A.M., Charpak, S., Lauritzen, M., MacVicar, B.A., Newman, E.A., 2010. Glial and neuronal control of brain blood flow. Nature 468, 232-243.

Attwell, D., Laughlin, S.B., 2001. An Energy Budget for Signaling in the Grey Matter of the Brain. Journal of Cerebral Blood Flow & Metabolism 21, 1133-1145.

Attwell, D., Mishra, A., Hall, C.N., O'Farrell, F.M., Dalkara, T., 2015. What is a pericyte? Journal of Cerebral Blood Flow & Metabolism, 0271678X15610340.

Barrett, M.J., Suresh, V., 2013. Extra permeability is required to model dynamic oxygen measurements: evidence for functional recruitment? Journal of Cerebral Blood Flow & Metabolism 33, 1402-1411.

Barrett, M.J.P., Suresh, V., 2015. Improving estimates of the cerebral metabolic rate of oxygen from optical imaging data. NeuroImage 106, 101-110.

Barrett, M.J.P., Tawhai, M.H., Suresh, V., 2012. Arteries dominate volume changes during brief functional hyperemia: evidence from mathematical modelling. NeuroImage 62, 482–492.

Blinder, P., Shih, A.Y., Rafie, C., Kleinfeld, D., 2010. Topological basis for the robust distribution of blood to rodent neocortex. Proceedings of the National Academy of Sciences 107, 12670-12675.

Blinder, P., Tsai, P.S., Kaufhold, J.P., Knutsen, P.M., Suhl, H., Kleinfeld, D., 2013. The cortical angiome: an interconnected vascular network with noncolumnar patterns of blood flow. Nature Neurosci 16, 889-897.

Boxerman, J.L., Bandettini, P.A., Kwong, K.K., Baker, J.R., Davis, T.L., Rosen, B.R., Weisskoff, R.M., 1995a. The intravascular contribution to fmri signal change: monte carlo modeling and diffusion-weighted studies in vivo. Magnetic Resonance in Medicine 34, 4-10.

Boxerman, J.L., Hamberg, L.M., Rosen, B.R., Weisskoff, R.M., 1995b. MR contrast due to intravascular magnetic susceptibility perturbations. Magn Reson Med 34, 555-566.

Buxton, R.B., 2001. The Elusive Initial Dip. NeuroImage 13, 953-958.

Buxton, R.B., 2013. The physics of functional magnetic resonance imaging (fMRI). Reports on Progress in Physics 76, 096601.

Buxton, R.B., Griffeth, V.E.M., Simon, A.B., Moradi, F., 2014. Variability of the coupling of blood flow and oxygen metabolism responses in the brain: a problem for interpreting BOLD studies but potentially a new window on the underlying neural activity. Brain Imaging Methods 8, 139.

Cassot, F., Frederic, L., Sylvie, L., Prasanna, P., Henri, D., 2009. Scaling Laws for Branching Vessels of Human Cerebral Cortex. Microcirculation 16, 331-344.

Chen, B.R., Bouchard, M.B., McCaslin, A.F., Burgess, S.A., Hillman, E.M., 2011. High-speed vascular dynamics of the hemodynamic response. NeuroImage 54, 1021-1030.

Chen, B.R., Kozberg, M.G., Bouchard, M.B., Shaik, M.A., Hillman, E.M., 2014. A critical role for the vascular endothelium in functional neurovascular coupling in the brain. Journal of the American Heart Association 3, e000787.
Chen, J.J., Pike, G.B., 2009. BOLD-specific cerebral blood volume and blood flow changes during neuronal activation in humans. NMR in Biomedicine 22, 1054–1062.
Chen, J.J., Pike, G.B., 2010. MRI measurement of the BOLD-specific flow-volume relationship during hypercapnia and hypocapnia in humans. NeuroImage 53, 383 - 391.
Cohen-Adad, J., Polimeni, J.R., Helmer, K.G., Benner, T., McNab, J.A., Wald, L.L., Rosen, B.R., Mainero, C., 2012. T2* mapping and B0 orientation-dependence at 7 T reveal cyto- and myeloarchitecture organization of the human cortex. NeuroImage 60, 1006-1014.
Davis, T.L., Kwong, K.K., Weisskoff, R.M., Rosen, B.R., 1998. Calibrated functional MRI: Mapping the dynamics of oxidative metabolism. Proceedings of the National Academy of Sciences of the United States of America 95, 1834-1839.
Devor, A., Hillman, E.M., Tian, P., Waeber, C., Teng, I.C., Ruvinskaya, L., Shalinsky, M.H., Zhu, H., Haslinger, R.H., Narayanan, S.N., others, 2008. Stimulus-induced changes in blood flow and 2-deoxyglucose uptake dissociate in ipsilateral somatosensory cortex. Journal of Neuroscience 28, 14347-14357.
Devor, A., Sakadzic, S., Saisan, P.A., Yaseen, M.A., Roussakis, E., Srinivasan, V.J., Vinogradov, S.A., Rosen, B.R., Buxton, R.B., Dale, A.M., Boas, D.A., 2011. "Overshoot" of O-2 Is Required to Maintain Baseline Tissue Oxygenation at Locations Distal to Blood Vessels. Journal of Neuroscience 31, 13676-13681.
Devor, A., Tian, P., Nishimura, N., Teng, I.C., Hillman, E.M., Narayanan, S., Ulbert, I., Boas, D.A., Kleinfeld, D., Dale, A.M., 2007. Suppressed neuronal activity and concurrent arteriolar vasoconstriction may explain negative blood oxygenation level-dependent signal. Journal of Neuroscience 27, 4452-4459.
Diemer, K., Henn, R., 1965. Kapillarvermehrung in der Hirnrinde der Rratte unter chronischem Sauerstoffmangel. Die Naturwissenschafter 52, 135-136.
Douglas, R.J., Martin, K.A., 2004. Neuronal circuits of the neocortex. Annu Rev Neurosci 27, 419-451.
Drew, P.J., Shih, A.Y., Kleinfeld, D., 2011. Fluctuating and sensory-induced vasodynamics in rodent cortex extend arteriole capacity. Proceedings of the National Academy of Sciences 108, 8473-8478.
Dunn, A.K., Devor, A., Bolay, H., Andermann, M.L., Moskowitz, M.A., Dale, A.M., Boas, D.A., 2003. Simultaneous imaging of total cerebral hemoglobin concentration, oxygenation, and blood flow during functional activation. Optics Letters 28, 28-30.
Dunn, A.K., Devor, A., Dale, A.M., Boas, D.A., 2005. Spatial extent of oxygen metabolism and hemodynamic changes during functional activation of the rat somatosensory cortex. NeuroImage 27, 279 - 290.
Duvernoy, H.M., Delon, S., Vannson, J.L., 1981. Cortical blood vessels of the human brain. Brain Res Bull 7, 519-579.
Erinjeri, J.P., Woolsey, T.A., 2002. Spatial integration of vascular changes with neural activity in mouse cortex. Journal of Cerebral Blood Flow & Metabolism 22, 353-360.
Erturk, A., Becker, K., Jahrling, N., Mauch, C.P., Hojer, C.D., Egen, J.G., Hellal, F., Bradke, F., Sheng, M., Dodt, H.U., 2012. Three-dimensional imaging of solvent-cleared organs using 3DISCO. Nat Protoc 7, 1983-1995.

Fernandez-Klett, F., Offenhauser, N., Dirnagl, U., Priller, J., Lindauer, U., 2010. Pericytes in capillaries are contractile in vivo, but arterioles mediate functional hyperemia in the mouse brain. Proc Natl Acad Sci U S A 107, 22290-22295.
Fernández-Klett, F., Priller, J., 2015. Diverse functions of pericytes in cerebral blood flow regulation and ischemia. Journal of Cerebral Blood Flow & Metabolism 35, 883-887.
Fink, J.R., Muzi, M., Peck, M., Krohn, K.A., 2015. Multimodality Brain Tumor Imaging: MR Imaging, PET, and PET/MR Imaging. Journal of Nuclear Medicine 56, 1554-1561.
Fonta, C., Imbert, M., 2002. Vascularization in the primate visual cortex during development. Cerebral Cortex 12, 199-211.
Fox, P.T., Raichle, M.E., 1986. Focal physiological uncoupling of cerebral blood flow and oxidative metabolism during somatosensory stimulation in human subjects. Proceedings of the National Academy of Sciences of the United States of America 83, 1140-1144.
Gagnon, L., Sakadžić, S., Lesage, F., Musacchia, J.J., Lefebvre, J., Fang, Q., Yücel, M.A., Evans, K.C., Mandeville, E.T., Cohen-Adad, J., Polimeni, J.a.R., Yaseen, M.A., Lo, E.H., Greve, D.N., Buxton, R.B., Dale, A.M., Devor, A., Boas, D.A., 2015. Quantifying the Microvascular Origin of BOLD-fMRI from First Principles with Two-Photon Microscopy and an Oxygen-Sensitive Nanoprobe. The Journal of Neuroscience 35, 3663-3675.
Goense, J., Merkle, H., Logothetis, N.K., 2012. High-resolution fMRI reveals laminar differences in neurovascular coupling between positive and negative BOLD responses. Neuron 76, 629-639.
Golub, A.S., Pittman, R.N., 2005. Erythrocyte-associated transients in Po2 revealed in capillaries of rat mesentery. American Journal of Physiology - Heart and Circulatory Physiology 288, H2735-H2743.
Guibert, R., Fonta, C., Plouraboue, F., 2010. Cerebral blood flow modeling in primate cortex. J Cereb Blood Flow Metab 30, 1860-1873.
Guibert, R., Fonta, C., Risser, L., Plouraboué, F., 2012. Coupling and robustness of intra-cortical vascular territories. NeuroImage 62, 408-417.
Gutiérrez-Jiménez, E., Cai, C., Mikkelsen, I.K.a., Rasmussen, P.M., Angleys, H., Merrild, M., Mouridsen, K., Jespersen, S.N., Lee, J., Iversen, N.K., others, 2016. Effect of electrical forepaw stimulation on capillary transit-time heterogeneity (CTH). Journal of Cerebral Blood Flow & Metabolism, 0271678X16631560.
Hall, C.N., Reynell, C., Gesslein, B., Hamilton, N.B., Mishra, A., Sutherland, B.A., O'Farrell, F.M., Buchan, A.M., Lauritzen, M., Attwell, D., 2014. Capillary pericytes regulate cerebral blood flow in health and disease. Nature 508, 55-60.
Hamilton, N.B., Attwell, D., Hall, C.N., 2010. Pericyte-mediated regulation of capillary diameter: a component of neurovascular coupling in health and disease. Front Neuroenergetics 2, 102-115.
Harik, S.I., Behmand, R.A., LaManna, J.C., 1994. Hypoxia increases glucose transport at blood-brain barrier in rats. J Appl Physiol 77, 896-901.
Hartmann, D.A., Underly, R.G., Grant, R.I., Watson, A.N., Lindner, V., Shih, A.Y., 2015. Pericyte structure and distribution in the cerebral cortex revealed by high-resolution imaging of transgenic mice. Neurophotonics 2, 041402-041402.
Heinzer, S., Krucker, T., Stampanoni, M., Abela, R., Meyer, E.P., Schuler, A., Schneider, P., Muller, R., 2006. Hierarchical microimaging for multiscale analysis of large vascular networks. NeuroImage 32, 626-636.
Heinzle, J., Koopmans, P.J., den Ouden, H.E.M., Raman, S., Stephan, K.E., 2016. A hemodynamic model for layered BOLD signals. NeuroImage 125, 556-570.

Hellums, J.D., 1977. The resistance to oxygen transport in the capillaries relative to that in the surrounding tissue. Microvasc Res 13, 131–136.
Hill, R.A., Tong, L., Yuan, P., Murikinati, S., Gupta, S., Grutzendler, J., 2015. Regional blood flow in the normal and ischemic brain is controlled by arteriolar smooth muscle cell contractility and not by capillary pericytes. Neuron 87, 95-110.
Hillman, E.M., 2014. Coupling mechanism and significance of the BOLD signal: a status report. Annual review of neuroscience 37, 161-181.
Hillman, E.M.C., Devor, A., Bouchard, M.B., Dunn, A.K., Krauss, G.W., Skoch, J., Bacskai, B.J., Dale, A.M., Boas, D.A., 2007. Depth-resolved optical imaging and microscopy of vascular compartment dynamics during somatosensory stimulation. NeuroImage 35, 89 - 104.
Hirano, Y., Stefanovic, B., Silva, A.C., 2011. Spatiotemporal evolution of the functional magnetic resonance imaging response to ultrashort stimuli. Journal of Neuroscience 31, 1440-1447.
Hirsch, S., Reichold, J., Schneider, M., Szekely, G., Weber, B., 2012. Topology and hemodynamics of the cortical cerebrovascular system. JCBFM 32, 952-967.
Ho, Y.-C.L., Petersen, E.T., Zimine, I., Golay, X., 2011. Similarities and Differences in Arterial Responses to Hypercapnia and Visual Stimulation. Journal of Cerebral Blood Flow & Metabolism 31, 560-571.
Hoge, R.D., Atkinson, J., Gill, B., Crelier, G.R., Marrett, S., Pike, G.B., 1999. Investigation of BOLD signal dependence on cerebral blood flow and oxygen consumption: The deoxyhemoglobin dilution model. Magnetic Resonance in Medicine 42, 849–863.
Hu, X., Yacoub, E., 2012. The story of the initial dip in fMRI. NeuroImage 62, 1103-1108.
Huber, L., Goense, J., Kennerley, A.J., Trampel, R., Guidi, M., Reimer, E., Ivanov, D., Neef, N., Gauthier, C.J., Turner, R., Möller, H.E., 2015. Cortical lamina-dependent blood volume changes in human brain at 7 T. NeuroImage 107, 23-33.
Huber, L., Ivanov, D., Handwerker, D.A., Marrett, S., Guidi, M., Uludağ, K., Bandettini, P.A., Poser, B.A., 2016. Techniques for blood volume fMRI with VASO: From low-resolution mapping towards sub-millimeter layer-dependent applications. NeuroImage.
Iadecola, C., Nedergaard, M., 2007. Glial regulation of the cerebral microvasculature. Nature neuroscience 10, 1369-1376.
Iadecola, C., Yang, G., Ebner, T.J., Chen, G., 1997. Local and propagated vascular responses evoked by focal synaptic activity in cerebellar cortex. Journal of neurophysiology 78, 651-659.
Iliff, J.J., Nedergaard, M., 2013. Is There a Cerebral Lymphatic System? Stroke 44, S93-S95.
Iliff, J.J., Wang, M.H., Liao, Y.H., Plogg, B.A., Peng, W.G., Gundersen, G.A., Benveniste, H., Vates, G.E., Deane, R., Goldman, S.A., Nagelhus, E.A., Nedergaard, M., 2012. A Paravascular Pathway Facilitates CSF Flow Through the Brain Parenchyma and the Clearance of Interstitial Solutes, Including Amyloid beta. Science Translational Medicine 4.
Iliff, J.J., Wang, M.H., Zeppenfeld, D.M., Venkataraman, A., Plog, B.A., Liao, Y.H., Deane, R., Nedergaard, M., 2013. Cerebral Arterial Pulsation Drives Paravascular CSF-Interstitial Fluid Exchange in the Murine Brain. Journal of Neuroscience 33, 18190-18199.
Itoh, Y., Suzuki, N., 2012. Control of brain capillary blood flow. Journal of Cerebral Blood Flow & Metabolism 32, 1167-1176.
Jespersen, S.N., Østergaard, L., 2012. The roles of cerebral blood flow, capillary transit time heterogeneity, and oxygen tension in brain oxygenation and metabolism. Journal of Cerebral Blood Flow and Metabolism 32, 264–277.

Jones, T.H., Morawetz, R.B., Crowell, R.M., Marcoux, F.W., FitzGibbon, S.J., DeGirolami, U., Ojemann, R.G., 1981. Thresholds of focal cerebral ischemia in awake monkeys. Journal of Neurosurgery 54, 773-782.
Kasischke, K.A., Lambert, E.M., Panepento, B., Sun, A., Gelbard, H.A., Burgess, R.W., Foster, T.H., Nedergaard, M., 2011. Two-photon NADH imaging exposes boundaries of oxygen diffusion in cortical vascular supply regions. Journal of Cerebral Blood Flow and Metabolism 31, 68–81.
Keller, A.L., Schüz, A., Logothetis, N.K., Weber, B., 2011. Vascularization of cytochrome oxidase-rich blobs in the primary visual cortex of squirrel and macaque monkeys. The Journal of Neuroscience 31, 1246-1253.
Kim, T., Hendrich, K.S., Masamoto, K., Kim, S.-G., 2007. Arterial versus total blood volume changes during neural activity-induced cerebral blood flow change: implication for BOLD fMRI. Journal of Cerebral Blood Flow and Metabolism 27, 1235–1247.
Kim, T., Kim, S.-G., 2010. Cortical layer-dependent arterial blood volume changes: Improved spatial specificity relative to BOLD fMRI. NeuroImage 49, 1340 - 1349.
Kim, T., Kim, S.-G., 2011. Temporal dynamics and spatial specificity of arterial and venous blood volume changes during visual stimulation: implication for BOLD quantification. Journal of Cerebral Blood Flow and Metabolism 31, 1211–1222.
Kleinfeld, D., Mitra, P.P., Helmchen, F., Denk, W., 1998. Fluctuations and stimulus-induced changes in blood flow observed in individual capillaries in layers 2 through 4 of rat neocortex. Proceedings of the National Academy of Sciences 95, 15741-15746.
Kwong, K.K., Belliveau, J.W., Chesler, D.A., Goldberg, I.E., Weisskoff, R.M., Poncelet, B.P., Kennedy, D.N., Hoppel, B.E., Cohen, M.S., Turner, R., et al., 1992. Dynamic magnetic resonance imaging of human brain activity during primary sensory stimulation. Proc Natl Acad Sci U S A 89, 5675-5679.
LaManna, J.C., Vendel, L.M., Farrell, R.M., 1992. Brain adaptation to chronic hypobaric hypoxia in rats. J Appl Physiol 72, 2238-2243.
Lauwers, F., Cassot, F., Lauwers-Cances, V., Puwanarajah, P., Duvernoy, H., 2008. Morphometry of the human cerebral cortex microcirculation: General characteristics and space-related profiles. NeuroImage 39, 936-948.
Lecoq, J., Parpaleix, A., Roussakis, E., Ducros, M., Houssen, Y.G., Vinogradov, S.A., Charpak, S., 2011. Simultaneous two-photon imaging of oxygen and blood flow in deep cerebral vessels. Nature medicine 17, 893–898.
Lee, J., Jiang, J.Y., Wu, W., Lesage, F., Boas, D.A., 2014. Statistical intensity variation analysis for rapid volumetric imaging of capillary network flux. Biomedical optics express 5, 1160-1172.
Lee, J., Wu, W., Boas, D.A., 2015. Early capillary flux homogenization in response to neural activation. Journal of Cerebral Blood Flow & Metabolism, 0271678X15605851.
Li, J., Bravo, D.S., Louise Upton, A., Gilmour, G., Tricklebank, M.D., Fillenz, M., Martin, C., Lowry, J.P., Bannerman, D.M., McHugh, S.B., 2011. Close temporal coupling of neuronal activity and tissue oxygen responses in rodent whisker barrel cortex. European Journal of Neuroscience 34, 1983-1996.
Lindvere, L., Janik, R., Dorr, A., Chartash, D., Sahota, B., Sled, J.G., Stefanovic, B., 2013. Cerebral microvascular network geometry changes in response to functional stimulation. NeuroImage 71, 248-259.

Lorthois, S., Cassot, F., Lauwers, F., 2011. Simulation study of brain blood flow regulation by intra-cortical arterioles in an anatomically accurate large human vascular network: Part I: Methodology and baseline flow. NeuroImage 54, 1031-1042.
Lücker, A., Weber, B., Jenny, P., 2015. A dynamic model of oxygen transport from capillaries to tissue with moving red blood cells. American Journal of Physiology - Heart and Circulatory Physiology 308, H206-H216.
Lyons, D.G., Parpaleix, A., Roche, M., Charpak, S., 2016. Mapping oxygen concentration in the awake mouse brain. Elife 5, e12024.
Markuerkiaga, I., Barth, M., Norris, D.G., 2016. A cortical vascular model for examining the specificity of the laminar BOLD signal. NeuroImage 132, 491-498.
Masamoto, K., Fukuda, M., Vazquez, A., Kim, S.-G., 2009. Dose-dependent effect of isoflurane on neurovascular coupling in rat cerebral cortex. European Journal of Neuroscience 30, 242-250.
Masamoto, K., Takizawa, N., Kobayashi, H., Oka, K., Tanishita, K., 2003. Dual responses of tissue partial pressure of oxygen after functional stimulation in rat somatosensory cortex. Brain research 979, 104 - 113.
Masamoto, K., Vazquez, A., Wang, P., Kim, S.-G., 2008. Trial-by-trial relationship between neural activity, oxygen consumption, and blood flow responses. NeuroImage 40, 442 - 450.
Mathiisen, T.M., Lehre, K.P., Danbolt, N.C., Ottersen, O.P., 2010. The perivascular astroglial sheath provides a complete covering of the brain microvessels: an electron microscopic 3D reconstruction. Glia 58, 1094-1103.
Mayhew, J., Johnston, D., Berwick, J., Jones, M., Coffey, P., Zheng, Y., 2000. Spectroscopic Analysis of Neural Activity in Brain: Increased Oxygen Consumption Following Activation of Barrel Cortex. NeuroImage 12, 664–675.
Menon, R.S., 2012. The great brain versus vein debate. Neuroimage 62, 970-974.
Miller, A.T., Jr., Hale, D.M., 1970. Increased vascularity of brain, heart, and skeletal muscle of polycythemic rats. Am J Physiol 219, 702-704.
Moon, C.H., Fukuda, M., Kim, S.-G., 2013. Spatiotemporal characteristics and vascular sources of neural-specific and -nonspecific fMRI signals at submillimeter columnar resolution. NeuroImage 64, 91-103.
Moskowitz, M.A., Lo, E.H., Iadecola, C., 2010. The science of stroke: mechanisms in search of treatments. Neuron 67, 181–198.
Mosso, A., 1881. Ueber den Kreislauf des Blutes im Menschlichen Gehirn, Leipzig.
Ngai, A.C., Ko, K.R., Morii, S., Winn, H.R., 1988. Effect of sciatic nerve stimulation on pial arterioles in rats. American Journal of Physiology-Heart and Circulatory Physiology 254, H133-H139.
Ngai, A.C., Winn, H.R., 2002. Pial arteriole dilation during somatosensory stimulation is not mediated by an increase in CSF metabolites. American Journal of Physiology-Heart and Circulatory Physiology 51, H902.
Nguyen, J., Nishimura, N., Fetcho, R.N., Iadecola, C., Schaffer, C.B., 2011. Occlusion of cortical ascending venules causes blood flow decreases, reversals in flow direction, and vessel dilation in upstream capillaries. Journal of Cerebral Blood Flow & Metabolism 31, 2243-2254.
Nishimura, N., Schaffer, C.B., Friedman, B., Lyden, P.D., Kleinfeld, D., 2007. Penetrating arterioles are a bottleneck in the perfusion of neocortex. Proceedings of the National Academy of Sciences 104, 365-370.

O'Herron, P., Chhatbar, P.Y., Levy, M., Shen, Z., Schramm, A.E., Lu, Z., Kara, P., 2016. Neural correlates of single-vessel haemodynamic responses in vivo. Nature advance online publication.
Ogawa, S., Lee, T.M., Kay, A.R., Tank, D.W., 1990. Brain magnetic resonance imaging with contrast dependent on blood oxygenation. Proceedings of the National Academy of Sciences of the United States of America 87, 9868-9872.
Ogawa, S., Menon, R.S., Tank, D.W., Kim, S.G., Merkle, H., Ellermann, J.M., Ugurbil, K., 1993. Functional brain mapping by blood oxygenation level-dependent contrast magnetic resonance imaging. A comparison of signal characteristics with a biophysical model. Biophysical Journal 64, 803–812.
Opitz, E., 1951. Increased vascularization of the tissue due to acclimati- zation to high altitude and its significance for the oxygen transport. Exp Med Surg 9, 389-403.
Parpaleix, A., Goulam Houssen, Y., Charpak, S., 2013. Imaging local neuronal activity by monitoring PO2 transients in capillaries. Nature medicine 19, 241–246.
Peppiatt, C.M., Howarth, C., Mobbs, P., Attwell, D., 2006. Bidirectional control of CNS capillary diameter by pericytes. Nature 443, 700-704.
Plouraboue, F., Cloetens, P., Fonta, C., Steyer, A., Lauwers, F., Marc-Vergnes, J.P., 2004. X-ray high-resolution vascular network imaging. J Microsc 215, 139-148.
Poplawsky, A.J., Fukuda, M., Murphy, M., Kim, S.-G., 2015. Layer-Specific fMRI Responses to Excitatory and Inhibitory Neuronal Activities in the Olfactory Bulb. The Journal of Neuroscience 35, 15263-15275.
Reichold, J., Stampanoni, M., Lena Keller, A., Buck, A., Jenny, P., Weber, B., 2009. Vascular graph model to simulate the cerebral blood flow in realistic vascular networks. J Cereb Blood Flow Metab 29, 1429-1443.
Reina-De La Torre, F., Rodriguez-Baeza, A., Sahuquillo-Barris, J., 1998. Morphological characteristics and distribution pattern of the arterial vessels in human cerebral cortex: a scanning electron microscope study. Anat Rec 251, 87-96.
Risser, L., Plouraboue, F., Cloetens, P., Fonta, C., 2009. A 3D-investigation shows that angiogenesis in primate cerebral cortex mainly occurs at capillary level. International Journal of Developmental Neuroscience 27, 185-196.
Roy, C.S., Sherrington, M.B., 1890. On the regulation of the blood-supply of the brain. Journal of Physiology London 11, 85-108.
Sakadžić, S., Mandeville, E.T., Gagnon, L., Musacchia, J.J., Yaseen, M.A., Yucel, M.A., Lefebvre, J., Lesage, F., Dale, A.M., Eikermann-Haerter, K., Ayata, C., Srinivasan, V.J., Lo, E.H., Devor, A., Boas, D.A., 2014. Large arteriolar component of oxygen delivery implies a safe margin of oxygen supply to cerebral tissue. Nature communications 5.
Sakadžić, S., Roussakis, E., Yaseen, M.A., Mandeville, E.T., Srinivasan, V.J., Arai, K., Ruvinskaya, S., Devor, A., Lo, E.H., Vinogradov, S.A., others, 2010. Two-photon high-resolution measurement of partial pressure of oxygen in cerebral vasculature and tissue. Nature Methods 7, 755-759.
Schaffer, C.B., Friedman, B., Nishimura, N., Schroeder, L.F., Tsai, P.S., Ebner, F.F., Lyden, P.D., Kleinfeld, D., 2006. Two-photon imaging of cortical surface microvessels reveals a robust redistribution in blood flow after vascular occlusion. PLoS Biol 4, e22.
Schmid, F., Reichold, J., Weber, B., Jenny, P., 2015. The impact of capillary dilation on the distribution of red blood cells in artificial networks. American Journal of Physiology-Heart and Circulatory Physiology 308, H733-H742.

Schmid, F., Tsai, P.S., Kleinfeld, D., Jenny, P., Weber, B., 2017. Depth-dependent flow and pressure characteristics in cortical microvascular networks. PLOS Computational Biology 13, e1005392.
Sekiguchi, Y., Takuwa, H., Kawaguchi, H., Kikuchi, T., Okada, E., Kanno, I., Ito, H., Tomita, Y., Itoh, Y., Suzuki, N., others, 2014. Pial arteries respond earlier than penetrating arterioles to neural activation in the somatosensory cortex in awake mice exposed to chronic hypoxia: an additional mechanism to proximal integration signaling? Journal of Cerebral Blood Flow & Metabolism 34, 1761-1770.
Shih, A.Y., Blinder, P., Tsai, P.S., Friedman, B., Stanley, G., Lyden, P.D., Kleinfeld, D., 2013. The smallest stroke: occlusion of one penetrating vessel leads to infarction and a cognitive deficit. Nature neuroscience 16, 55-63.
Shih, A.Y., Rühlmann, C., Blinder, P., Devor, A., Drew, P.J., Friedman, B., Knutsen, P.M., Lyden, P.D., Mateo, C., Mellander, L., others, 2015. Robust and fragile aspects of cortical blood flow in relation to the underlying angioarchitecture. Microcirculation 22, 204-218.
Souillard-Scemama, R., Tisserand, M., Calvet, D., Jumadilova, D., Lion, S., Turc, G., Edjlali, M., Mellerio, C., Lamy, C., Naggara, O., Meder, J.-F., Oppenheim, C., 2015. An update on brain imaging in transient ischemic attack. Journal of Neuroradiology 42, 3-11.
Stefanovic, B., Hutchinson, E., Yakovleva, V., Schram, V., Russell, J.T., Belluscio, L., Koretsky, A.P., Silva, A.C., 2008. Functional reactivity of cerebral capillaries. J Cereb Blood Flow Metab 28, 961-972.
Thompson, J.K., Peterson, M.R., Freeman, R.D., 2003. Single-Neuron Activity and Tissue Oxygenation in the Cerebral Cortex. Science 299, 1070-1072.
Tian, P., Teng, I.C., May, L.D., Kurz, R., Lu, K., Scadeng, M., Hillman, E.M., De Crespigny, A.J., D'Arceuil, H.E., Mandeville, J.B., others, 2010. Cortical depth-specific microvascular dilation underlies laminar differences in blood oxygenation level-dependent functional MRI signal. Proceedings of the National Academy of Sciences 107, 15246-15251.
Tieman, S.B., Mollers, S., Tieman, D.G., White, J., 2004. The blood supply of the cat's visual cortex and its postnatal development. Brain Res 998, 100-112.
Tsai, P.S., Friedman, B., Ifarraguerri, A.I., Thompson, B.D., Lev-Ram, V., Schaffer, C.B., Xiong, Q., Tsien, R.Y., Squier, J.A., Kleinfeld, D., 2003. All-optical histology using ultrashort laser pulses. Neuron 39, 27-41.
Tsai, P.S., Kaufhold, J.P., Blinder, P., Friedman, B., Drew, P.J., Karten, H.J., Lyden, P.D., Kleinfeld, D., 2009. Correlations of neuronal and microvascular densities in murine cortex revealed by direct counting and colocalization of nuclei and vessels. The Journal of Neuroscience 29, 14553-14570.
Turner, R., 2016. Uses, misuses, new uses and fundamental limitations of magnetic resonance imaging in cognitive science. Phil. Trans. R. Soc. B 371, 20150349.
Uhlirova, H., Kılıç, K., Tian, P., Sakadžić, S., Gagnon, L., Thunemann, M., Desjardins, M., Saisan, P.A., Nizar, K., Yaseen, M.A., Hagler, D.J., Vandenberghe, M., Djurovic, S., Andreassen, O.A., Silva, G.A., Masliah, E., Kleinfeld, D., Vinogradov, S., Buxton, R.B., Einevoll, G.T., Boas, D.A., Dale, A.M., Devor, A., 2016a. The roadmap for estimation of cell-type-specific neuronal activity from non-invasive measurements. Phil. Trans. R. Soc. B 371, 20150356.
Uhlirova, H., Kılıç, K., Tian, P., Thunemann, M., Desjardins, M., Saisan, P.A., Sakadžić, S., Ness, T.V., Mateo, C., Cheng, Q., others, 2016b. Cell type specificity of neurovascular coupling in cerebral cortex. Elife 5, e14315.

Uludağ, K., Blinder, P., 2017. Linking brain vascular physiology to hemodynamic response in ultra-high field MRI. NeuroImage.
Vazquez, A.L., Fukuda, M., Tasker, M.L., Masamoto, K., Kim, S.-G., 2010. Changes in cerebral arterial, tissue and venous oxygenation with evoked neural stimulation: implications for hemoglobin-based functional neuroimaging. Journal of Cerebral Blood Flow and Metabolism 30, 428–439.
Vazquez, A.L., Masamoto, K., Kim, S.-G., 2008. Dynamics of oxygen delivery and consumption during evoked neural stimulation using a compartment model and CBF and tissue PO2 measurements. NeuroImage 42, 49–59.
Vovenko, E., 1999. Distribution of oxygen tension on the surface of arterioles, capillaries and venules of brain cortex and in tissue in normoxia: an experimental study on rats. Pflugers Archiv (European Journal of Physiology) 437, 617–623.
Weber, B., Keller, A.L., Reichold, J., Logothetis, N.K., 2008. The microvascular system of the striate and extrastriate visual cortex of the macaque. Cerebral Cortex 18, 2318-2330.
Wei, Helen S., Kang, H., Rasheed, I.-Yar D., Zhou, S., Lou, N., Gershteyn, A., McConnell, Evan D., Wang, Y., Richardson, Kristopher E., Palmer, Andre F., Xu, C., Wan, J., Nedergaard, M., 2016. Erythrocytes Are Oxygen-Sensing Regulators of the Cerebral Microcirculation. Neuron 91, 851-862.
Xie, L.L., Kang, H.Y., Xu, Q.W., Chen, M.J., Liao, Y.H., Thiyagarajan, M., O'Donnell, J., Christensen, D.J., Nicholson, C., Iliff, J.J., Takano, T., Deane, R., Nedergaard, M., 2013. Sleep Drives Metabolite Clearance from the Adult Brain. Science 342, 373-377.
Xue, S., Gong, H., Jiang, T., Luo, W., Meng, Y., Liu, Q., Chen, S., Li, A., 2014. Indian-ink perfusion based method for reconstructing continuous vascular networks in whole mouse brain. PLoS One 9, e88067.
Yablonskiy, D.A., Haacke, E.M., 1994. Theory of NMR signal behavior in magnetically inhomogeneous tissues: The static dephasing regime. Magnetic Resonance in Medicine 32, 749-763.
Yao, J., Wang, L., Yang, J.-M., Maslov, K.I., Wong, T.T.W., Li, L., Huang, C.-H., Zou, J., Wang, L.V., 2015. High-speed label-free functional photoacoustic microscopy of mouse brain in action. Nature Methods advance online publication.
Yaseen, M.A., Srinivasan, V.J., Sakadzic, S., Radhakrishnan, H., Gorczynska, I., Wu, W., Fujimoto, J.G., Boas, D.A., 2011. Microvascular oxygen tension and flow measurements in rodent cerebral cortex during baseline conditions and functional activation. Journal of Cerebral Blood Flow and Metabolism 31, 1051–1063.
Zhang, E.T., Inman, C.B.E., Weller, R.O., 1990. Interrelationships of the Pia Mater and the Perivascular (Virchow-Robin) Spaces in the Human Cerebrum. Journal of Anatomy 170, 111-123.
Zhao, F., Wang, P., Hendrich, K., Ugurbil, K., Kim, S.-G., 2006. Cortical layer-dependent BOLD and CBV responses measured by spin-echo and gradient-echo fMRI: insights into hemodynamic regulation. NeuroImage 30, 1149-1160.
Zheng, D., LaMantia, A.S., Purves, D., 1991. Specialized vascularization of the primate visual cortex. J Neurosci 11, 2622-2629.